A design strategy to generate a SARS-CoV-2 RBD vaccine that abrogates ACE2 binding and improves neutralizing antibody responses

Jackson ImmunoResearch LABORATORIES INC.

ANTIBODIES FOR SEROLOGY AND DIAGNOSTICS

NEW

Anti-Human IgE Antibodies

For high-specificity immunoassay design and performance

Learn more

European Journal of Immunology

Immunity to infection

Basic

Rapid Research Article

A design strategy to generate a SARS-CoV-2 RBD vaccine that abrogates ACE2 binding and improves neutralizing antibody responses

Christoph Ratswohl[#1,2], *Clara Vázquez García*[1,3], *Ata ul Wakeel Ahmad*[1,3], *Hannes Gonschior*[4], *Mikhail Lebedin*[1,3], *Casper Ewijn Silvis*[1,3], *Lisa Spatt*[1], *Cathrin Gerhard*[1], *Martin Lehmann*[4], *Leif E. Sander*[3,6], *Florian Kurth*[3], *Simon Olsson*[5] and *Kathrin de la Rosa*[1,6]

1st time author
Read more about EJI's first-time authors

[1] Max Delbrück Center for Molecular Medicine in the Helmholtz Association (MDC), Berlin, Germany
[2] Department of Biology, Chemistry and Pharmacy, Free University of Berlin, Berlin, Germany
[3] Charité - Universitätsmedizin, Berlin, Germany
[4] Leibniz-Forschungsinstitut für Molekulare Pharmakologie (FMP), Berlin, Germany
[5] Department of Computer Science and Engineering, Chalmers University of Technology, Göteborg, Västra Götalands län, Sweden
[6] Berlin Institute of Health (BIH) at Charité, Berlin, Germany

The structure-based design of antigens holds promise for developing vaccines with higher efficacy and improved safety profiles. We postulate that abrogation of host receptor interaction bears potential for the improvement of vaccines by preventing antigen-induced modification of receptor function as well as the displacement or masking of the immunogen. Antigen modifications may yet destroy epitopes crucial for antibody neutralization. Here, we present a methodology that integrates deep mutational scans to identify and score SARS-CoV-2 receptor binding domain variants that maintain immunogenicity, but lack interaction with the widely expressed host receptor. Single point mutations were scored in silico, validated in vitro, and applied in vivo. Our top-scoring variant receptor binding domain-G502E prevented spike-induced cell-to-cell fusion, receptor internalization, and improved neutralizing antibody responses by 3.3-fold in rabbit immunizations. We name our strategy BIBAX for body-inert, B-cell-activating vaccines, which in the future may be applied beyond SARS-CoV-2 for the improvement of vaccines by design.

Keywords: BIBAX · Body-inert B-cell-activating vaccines · Receptor-binding abrogation · SARS-CoV-2 vaccine · Vaccine design

Additional supporting information may be found online in the Supporting Information section at the end of the article.

Correspondence: Dr. Kathrin de la Rosa
e-mail: Kathrin.delaRosa@mdc-berlin.de

[#]First-time first author: Christoph Ratswohl

Introduction

Many vaccines contain virus components that mediate pathogen entry into host cells and are targets for the elicitation of neutralizing antibodies [1]. Host receptors capable of binding to vaccine antigens can be widely expressed in different tissues and on distinct cell types including immune cells. Some host receptors are furthermore released by proteolytic cleavage and abundantly circulate in the body. We suggest that the binding of vaccines to membrane-bound and soluble receptors limit antigen availability through vaccine displacement or masking, thereby restricting immune responses. In fact, binding of antigens by pre-existing or ectopically applied antibodies can downregulate the maturation of B cells specific for the covered epitope through masking, which is independent of the fragment crystallizable (Fc) effector function [2–5]. Similarly, the antigen availability of factor H binding protein, which is a component of vaccines licensed for serogroup B meningococcus, was shown to be limited by the interaction with the highly abundant serum protein factor H (fH) [6, 7]. Apart from soluble receptors, membrane-bound receptors expressed in the tissue or on immune cells may further contribute to limited antigen availability. Consequently, the abrogation of receptor binding may be a general strategy to assist immune responses by ensuring immune recognition of relevant antigens and their epitopes. In addition, host receptors can represent key regulators of homeostasis through their enzymatic activity or by initiating signaling cascades. The interaction of a vaccine with a receptor may therefore impact regulatory functions, which could contribute to side effects. Hence, the efficacy and the safety of a vaccine may profit from the abrogation of host receptor interaction.

We here present a novel structure-based design strategy using the SARS-CoV-2 spike as a model antigen. SARS-CoV-2 spike binds with high affinity to the angiotensin-converting enzyme 2 (ACE2) receptor [8]. ACE2 is a key component of the renin–angiotensin system, contributing to the regulation of blood pressure and inflammation [9]. Furthermore, ACE2 is widely expressed by distinct cells and in various tissues including cardiomyocytes, the vasculature, and renal tubules [10]. As the ACE2 receptor can be cleaved by proteases [11], soluble ACE2 circulates in the blood and was found to be highly elevated in patients suffering from COVID-19 [12–16]. We, therefore, aim for a SARS-CoV-2 vaccine incapable of binding ACE2 to exclude dysregulation of ACE2-dependent vasoconstrictive and inflammatory processes and to avoid the displacement of the immunogen by ACE2-expressing cells.

Antibodies that potently neutralize SARS-CoV-2 can interfere with virus entry through interaction with the receptor binding motif (RBM), a part of the receptor binding domain (RBD) of the spike protein [17–19]. As mutating the RBM bears the risk of modifying immune-relevant epitopes, we employed an in silico strategy that allows the ranking of vaccine candidates by three main criteria: (1) minimizing host receptor interaction, (2) maintaining immune-relevant epitopes of neutralizing antibodies, and (3) retaining immunogen expression and stability. By validating identified candidates, we show in vitro that our strategy holds promise to ameliorate side effects and that it improves antibody responses *in vivo*. By presenting the development of a prototype vaccine for SARS-CoV-2, we introduce our strategy called BIBAX, which stands for body-inert, B-cell-activating vaccines.

Results

In silico identification of BIBAX candidates

To identify amino acid residues that are relevant for ACE2 binding and at the same time represent subdominant epitopes for antibodies, we integrated two sources of available deep mutational scanning data provided by Bloom and colleagues: first, receptor binding maps that systematically revealed RBD residues involved in ACE2 interaction; second, amino acid exchange maps of the RBD to identify mutations that favor an escape from antibody binding [20–23]. In addition, structural data supported the identification of antibody-antigen interaction hotspots. We scored amino acid exchanges according to their ability to interfere with receptor binding, contribute to antibody escape (Fig. 1A), and impact protein expression as a proxy for protein stability (Fig. 1B). We integrated the three parameters into a feasibility score (see Materials and methods section) and ranked all variants. The top 38 candidates represented amino acid exchanges at positions G502, Y505, L455, Y489, F456, Q498, S373, F486, and Y449 (Fig. 1C). Top hits were most frequently detected for G502, Y505, and L455 with 18, 5, and 3 amino acid exchanges, respectively. G502E, G502D, and Y505G represented the top three scoring candidates. Mapping all scores onto the RBD structure revealed that one edge of the ACE2 binding footprint of the RBD, including the two amino acids G502 and Y505, is particularly suited for BIBAX design modifications (Fig. 1D).

In vitro validation of in silico scorings

To validate our findings *in vitro*, we recombinantly produced RBD variants of high (dark red), medium (red), and negligible score (light red; Fig. 2A and Supporting information Figs. S1 and 2A) to test binding to ACE2 and SARS-CoV-2 neutralizing antibodies (nAbs) of classes 1–4 [24] in ELISA. As expected, G502E (total score 4.8) completely abrogated ACE2 binding, while maintaining binding of all tested nAbs. By contrast, L455R (total score 3.1) partially abrogated ACE2 binding - by 71% compared with WT - but also weakened interaction with three out of six class 1 and 2 nAbs, namely P2C-1F11 [25], REGN10933 [26], and C144 [27]. Class 3 and 4 nAbs were not affected by the L455R mutation. E484K (total score −2.9) had no significant impact on receptor binding while binding of three out of six class 1 and 2 nAbs was reduced or lost (Fig. 2B). Biolayer Interferometry (BLI) measurements confirmed a complete loss of receptor binding for G502E, while a partial and no loss were observed for L455R (K_D 54 nM, K_{on} 1.96 × 10^4 Ms^{-1}, K_{off} 1.07 × 10^{-3} s^{-1}) and E484K (K_D 3.2 nM, K_{on} 2.81 × 10^4 Ms^{-1}, K_{off} 8.96 × 10^{-5} s^{-1}) compared with WT (K_D 3.8 nM, K_{on} 2.28 × 10^4 Ms^{-1}, K_{off} 8.70

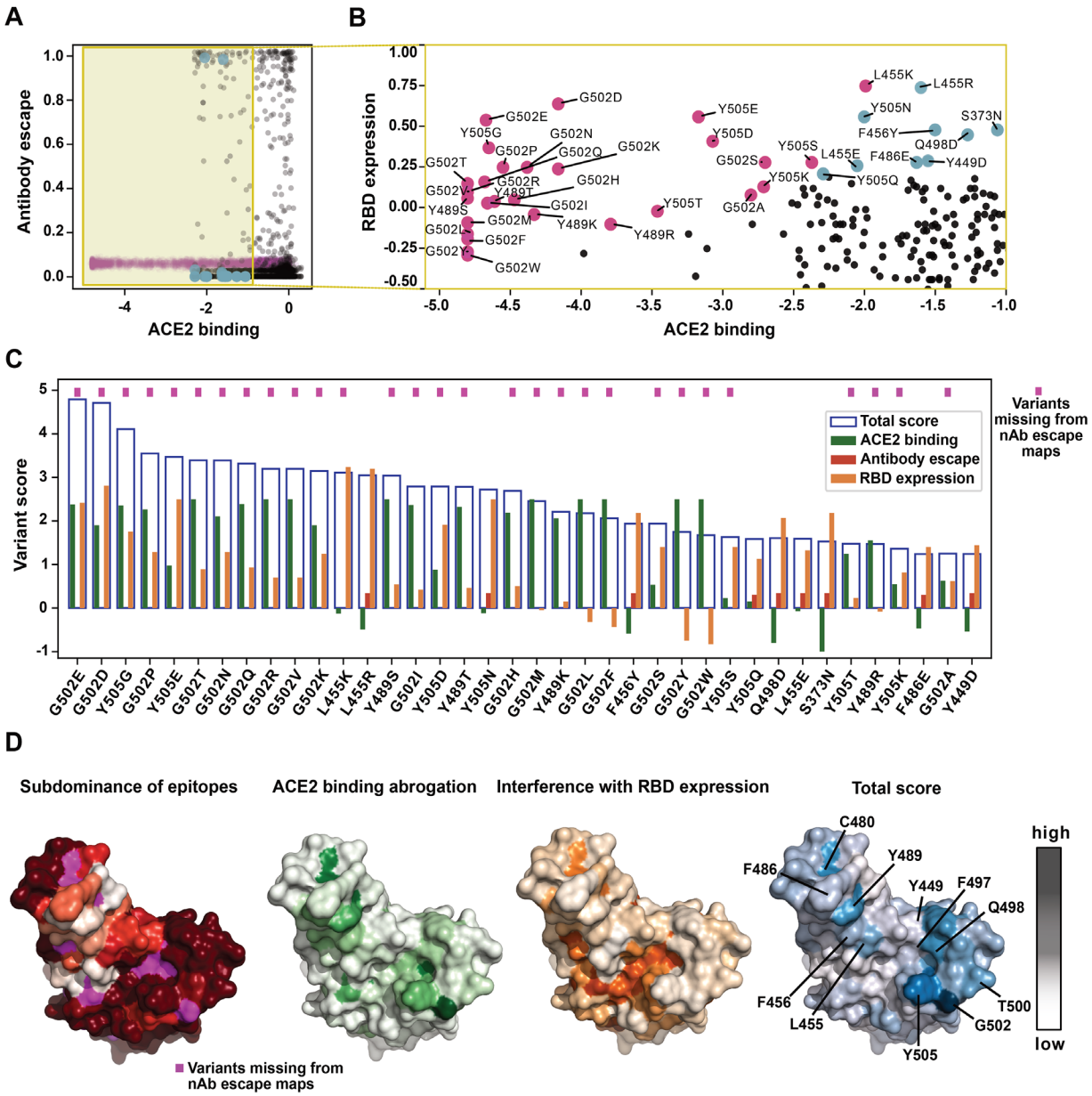

Figure 1. An in silico approach to identify immunocompetent, host receptor-evading antigens. (A) Scatter plot of SARS-CoV-2 RBD:ACE2 binding and neutralizing antibody (nAb) escape scores obtained from deep mutational scanning (MS) data [20–23]. Blue dots indicate variants fulfilling feasibility constraints for all three criteria, pink dots indicate variants lacking scores for nAb escape published in [20–23], and yellow transparent rectangle visualizes RBD residues considered for further downstream processes. Note, all pink values are scattered around their imputed value with normal noise ($\sigma = 0.01$) for visual clarity. (B) Scatter plot of SARS-CoV-2 RBD expression and SARS-CoV-2 RBD:ACE2 binding for variants preselected in (A); pink and blue dots correspond to highly scoring variants. (C) Total feasibility scores (blue bars) computed by individual contributions from ACE2 binding (green), antibody escape (red), and RBD expression (orange). The top 38 candidates are depicted from higher (left) to lower scores (right). (D) Individual contributions and total scores from all variants were pooled for each locus and mapped onto the RBD structure. Subdominance of epitopes is represented from dark to light red (higher to lower scores). The loss of ACE2 binding is depicted via dark to light green, positions where amino acid changes interfered with RBD expression are shown from dark to light orange. Total scores that combine all three contributions are displayed from dark to light blue. ACE2, angiotensin-converting enzyme 2; RBD, receptor binding domain.

$\times 10^{-5}$ s^{-1}), respectively (Supporting information Fig. S2B). To test a broader set of RBD variants in vitro, we focused on three selected class 1 and class 2 nAbs, namely CC12.1 [28], P2C-1F11, and REGN10933, whose epitopes overlap with the ACE2 binding interface (Supporting information Fig. S3). The binding data accurately reflected the gradient scores obtained from the in silico ranking (Fig. 2C). As a remarkable number of G502 amino acid exchanges obtained high scores *in silico*, we tested all possible amino acid exchanges at position G502 in vitro and obtained high performance for all variants except G502K, G502L, and G502F, which slightly affected nAb or ACE2 binding (Fig. 2D).

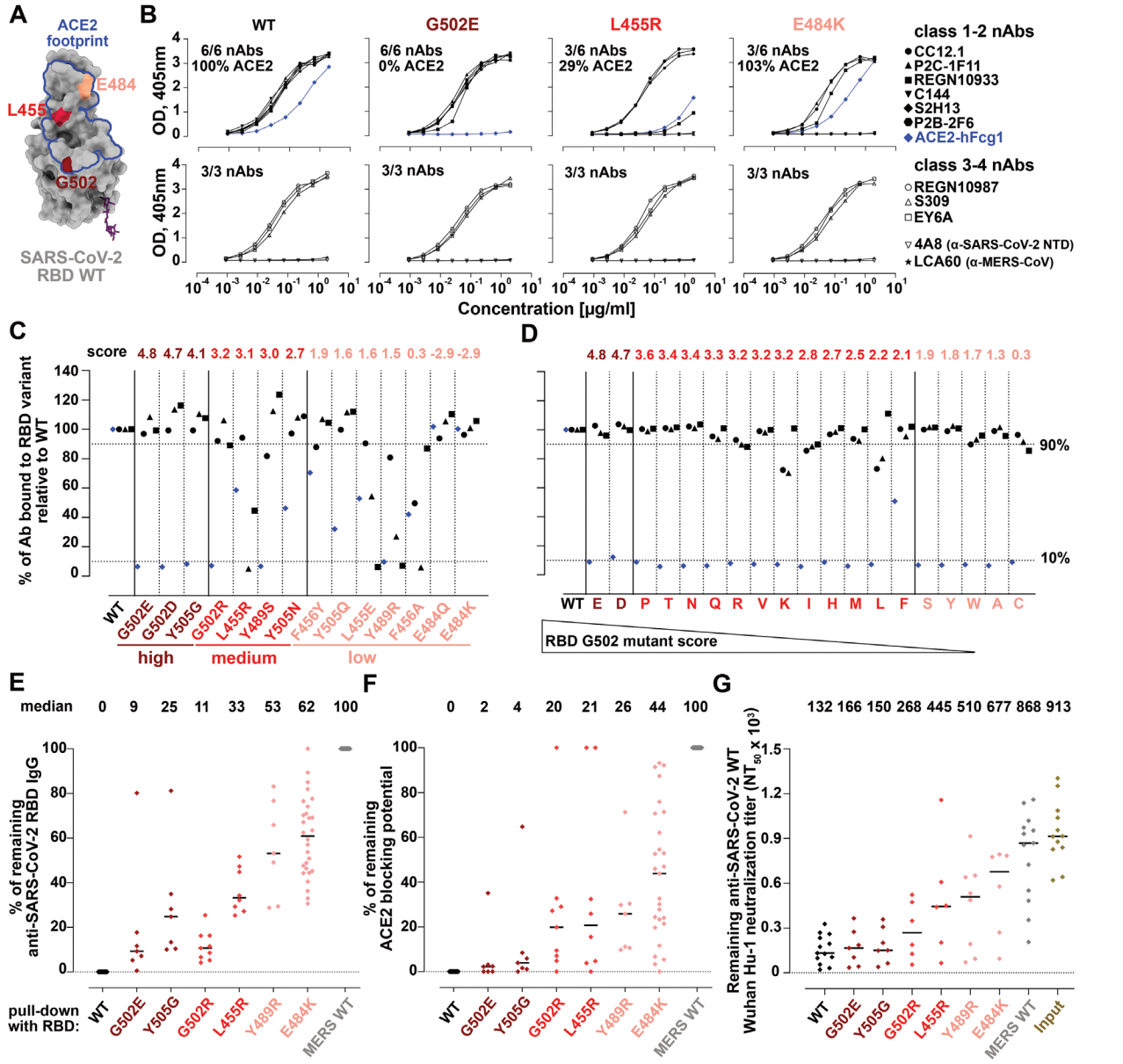

Figure 2. Confirming ACE2 binding abrogation and preservation of nAb epitopes of selected RBD variants in vitro. (A) Molecular surface representation of SARS-CoV-2 RBD WT. The ACE2 binding footprint (blue) and representative residues with high (dark red), medium (red) and low (light red) in silico scores are highlighted. (B) RBD WT and three representative RBD variants were tested in ELISA for binding to ACE2-hFcg1, class 1 and 2 nAbs (upper panel), and class 3 and 4 nAbs (lower panel). Anti-spike NTD 4A8 antibody as well as anti-MERS CoV antibody LCA60 served as negative controls. Shown are OD curves at 405 nm, the number of remaining nAbs bound as well as % of ACE2 binding compared with WT. OD, 405 nm, optical density for wavelength at 405 nm. (C) Subsets of RBD variants from each score group were tested in ELISA for binding to class 1 antibodies CC12.1 (circle), P2C-1F11 (triangle), REGN10933 (square), and ACE2-hFcg1 (diamond), with % of binding relative to RBD WT indicated. (D) The top scoring RBD residue G502 (WT) was exchanged to all possible amino acids, here organized by score. Shown is the % of nAb and ACE2-hFcg1 binding compared with RBD WT. (E–G) Sera from moderate ($n = 17$) and severe ($n = 17$) COVID-19 patients were cleared by pull-down with indicated RBD variants. Binding of remaining IgG to RBD WT (E) and blocking of ACE2 binding to RBD WT (F) were tested in ELISA and depicted as % of binding related to the SARS-CoV-2 RBD WT positive and MERS RBD WT negative pull-down controls. Remaining potential to neutralize SARS-CoV-2 WT Wuhan Hu-1 pseudotyped viruses (PsV) (G) is represented as half-maximum neutralization titer (NT_{50}) after pull-down with indicated variants. PsV neutralization assays were performed in technical duplicates with ACE2-hFcg1 as a standard. Median is shown. ACE2, angiotensin-converting enzyme 2; RBD, receptor binding domain.

Binding of selected recombinant antibodies does not represent the breadth of a polyclonal antibody response elicited after natural virus exposure or vaccination. Therefore, we aimed to address subdominance of selected residues on the RBD. An ordinary ELISA setting measuring binding of COVID-19 serum antibodies to the RBD failed to verify differences between the RBD variants (Supporting information Fig. S4A). We therefore made use of a different approach, by coupling selected RBDs with distinct in silico

scores to beads and conducting a serum pull-down (Supporting information Fig. S4B). We measured the reactivity of remaining antibodies in the supernatant to RBD WT, thus evaluating the antibody capture potential of each RBD variant. Of note, the high score variant G502E performed most similar to the RBD WT and efficiently captured antibodies that (1) bind to the RBD (Fig. 2E), (2) block RBD binding to ACE2 (Fig. 2F), and (3) neutralize virus particles pseudotyped with the SARS-CoV-2 spike (Fig. 2G). Interestingly, the high-scoring Y505G variant pulled down RBD-specific antibodies less efficiently than the medium-scorer G502R. However, Y505G outperformed G502R in its capacity to capture antibodies that block ACE2 binding to the RBD. Overall, a lower score was associated with less efficient depletion of antibodies from serum. Collectively, our data show that G502 and Y505 are subdominant sites that are poorly targeted by functionally relevant, polyclonal antibodies.

Spike variants lacking ACE2 binding prevent cell-to-cell fusion and antigen uptake

Antigens that change to a postfusion conformation bear the risk to induce antibodies recognizing a protein conformation irrelevant for neutralization. Furthermore, surface expression of fusion-competent antigens may cause side effects through the formation of syncytia that contribute to tissue damage in COVID-19 [29]. To demonstrate that receptor binding abrogation effectively prevents fusion, we expressed the transmembrane spike variants either in HEK293T cells, later mixed with ACE2-eGFP-transfected HEK293T cells, or in Vero E6 cells, which endogenously express ACE2 (Fig. 3A and B). Although similar levels of spike proteins were expressed on the cell surface (Supporting information Fig. S5A and B), G502E and G502R completely abrogated the fusogenic activity, whereas the variants L455R and E484K maintained the ability to fuse cells. Similar to receptor binding abrogation, spike-stabilizing substitutions of two prolines (2P) potently prevented the fusogenic activity of the spike (Fig. 3C and D). Of note, the 2P modification has already been introduced into approved SARS-CoV-2 vaccines [30]. Therefore, our data suggest that abrogation of receptor binding represents an alternative strategy to prefusion stabilization for avoiding vaccine-induced syncytia formation.

Spike binding to the ACE2 receptor induces internalization [31, 32] and a loss of ACE2 promotes tissue injury [33]. We, therefore, addressed if the G502E variant can abrogate cellular uptake of the spike via live-cell imaging. Fluorescently labeled, prefusion stabilized SARS-CoV-2 spike proteins were adsorbed by and internalized into Vero E6 cells within 90 min (Fig. 4A and B). The G502E variant significantly reduced and delayed the uptake of the spike by several hours but failed to abrogate internalization. Vero E6 cells treated with recombinant RBD bearing the G502E mutation showed almost no internalization even after 9 h of incubation (Supporting information Fig. S5C and D). This suggests that, aside from ACE2, additional receptors mediate the uptake of the full spike. Furthermore, spike WT internalization was observed in all cells by microscopy, whereas only 40–60% of cells bound a fluorescently labeled RBD or spike in FACS analysis (Supporting information Fig. S5B), further suggesting that additional low-affinity interactions contribute to the spike uptake during long-term incubation. It was lately reported that the monomeric RBD and the trimeric full spike protein of SARS-CoV-2 carry one and nine binding sites recognizing cellular heparan sulfates (HS), respectively, which can contribute to viral uptake [34, 35]. Hence, we addressed internalization of the spike in the presence of heparin. Indeed, heparin treatment reduced spike uptake as well as the number of cells gaining fluorescence (Fig. 4C). Similar results were observed for the G502E spike. Therefore, the G502E mutation abolishes ACE2-mediated uptake, whereas partial internalization of the spike remains through other receptor interactions such as HS. Collectively, our in vitro data suggest that a BIBAX antigen design prevents cell-to-cell fusion, loss of functional receptors from the cell surface, and clearance of antigen through receptor-mediated internalization.

BIBAX SARS-CoV-2 vaccines elicit high titers of neutralizing antibodies

To assess the immunogenicity of the G502E spike variant, we immunized 6 groups of female New Zealand white rabbits with two doses of 0.1, 1, and 10 μg recombinant spike with adjuvant (Fig. 5A). All immunizations were conducted with HexaPro spike, which is an improved version of the prefusion stabilized SARS-CoV-2 2P spike [36]. Although SARS-CoV-2 spike WT does not bind to mouse ACE2 [37], we observed binding to rabbit ACE2 (rbACE2) in ELISA and BLI assays to be two-fold reduced compared with human ACE2 (hACE2; K_D 3.8 nM, K_{on} 2.28×10^4 Ms^{-1}, K_{off} 8.70×10^{-5} s^{-1} vs. rbACE2 K_D 6.7 nM, K_{on} 2.96×10^4 Ms^{-1}, K_{off} 1.97×10^{-4} s^{-1}; Fig. 5B and C). Prior to immunization, the quantity and quality of all protein variants were determined to ensure comparability (Supporting information Fig. S6A). Titers of spike-specific IgG and neutralization potential were not significantly different between immunizations with the spike WT and the spike G502E mutant (Fig. 5D and Supporting information Fig. S6D–G). We postulated that ACE2 binding may skew the antibody response toward the N-terminal domain (NTD) that, together with the RBD, forms the globular head of the SARS-CoV-2 spike. Indeed, we observed more RBD over NTD reactive antibodies for G502E but not for WT immunizations (Fig. 5E). Furthermore, so-called class 1 antibodies recognizing part of the RBM were more frequent after G502E immunizations, as suggested by the depletion of rabbit sera with a mutant RBD containing an L455R mutation (Fig. 5F and G). Our data therefore confirm that neutralizing antibody responses are not compromised by receptor abrogating mutations and may focus the immune response toward the RBD if the spike is used as an immunogen.

Structural studies of the prefusion stabilized spike with a furin cleavage site substitution revealed that 67% of spike particles have either one or two RBDs in "up" conformation, capable of binding ACE2 [38]. Consequently, the majority of RBDs presented

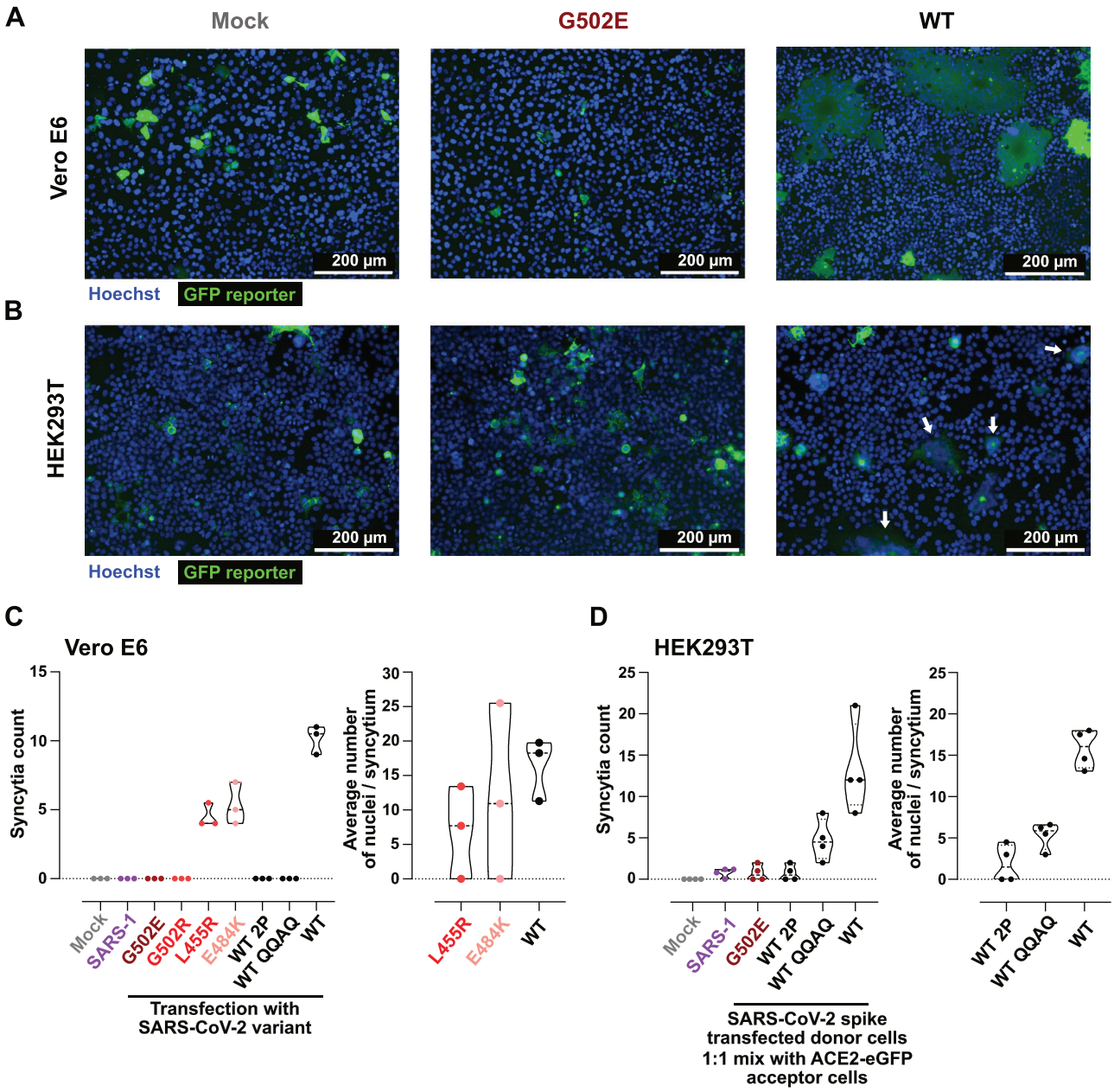

Figure 3. Loss of receptor binding reduces the fusogenic potential of the SARS-CoV-2 spike. (A) Vero E6 cells were transfected with indicated plasmid constructs to express transmembrane spike variants together with a GFP reporter to visualize fused cells. Syncytia formation from technical triplicates was determined after 48 h. GFP is shown in green and Hoechst-stained nuclei in blue. Scale bars = 200 µm. (B) ACE2-eGFP expressing HEK293T cells were mixed with SARS-CoV-2 spike variant expressing cells and monitored for cell-to-cell fusion events (white arrows). Technical duplicates were performed and two positions of each were analyzed after 24 h. ACE2-eGFP expression is displayed in green and nuclei were stained with Hoechst dye. Scale bars, 200 µm. (C, D) The syncytia count as well as the average number of nuclei per syncytium were determined from images (shown representatively in (A) and (B)) of Vero E6 (C) and ACE2-eGFP expressing HEK293T cells (D) at 10× magnification. Violin plots show the median with 75 and 25% percentiles. ACE2, angiotensin-converting enzyme 2; eGFP, enhanced green fluorescent protein.

on the spike are in a "down" state and, while incapable of binding ACE2, are able to elicit antibodies to exposed epitopes of the RBD, so-called class 2 and class 3 sites [24]. Therefore, we next addressed antibody responses when using RBD as an immunogen, as all molecules would be capable of interacting with the host receptor. The amount of applied protein was increased to 40 µg/shot to exclude that the benefits on antigen availability of a BIBAX design could be easily overcome by scaling up the dose of the immunogen (Fig. 6A). Apart from G502E, we also tested the lower scoring variants Y505G and G502R. These two variants efficiently abrogated host receptor binding but underperformed in the RBD capture assay, indicative of a reduced capability of eliciting neutralizing antibodies. Indeed, only after G502E immunization, RBD reactive IgG tended to be elevated (ED_{50} G502E

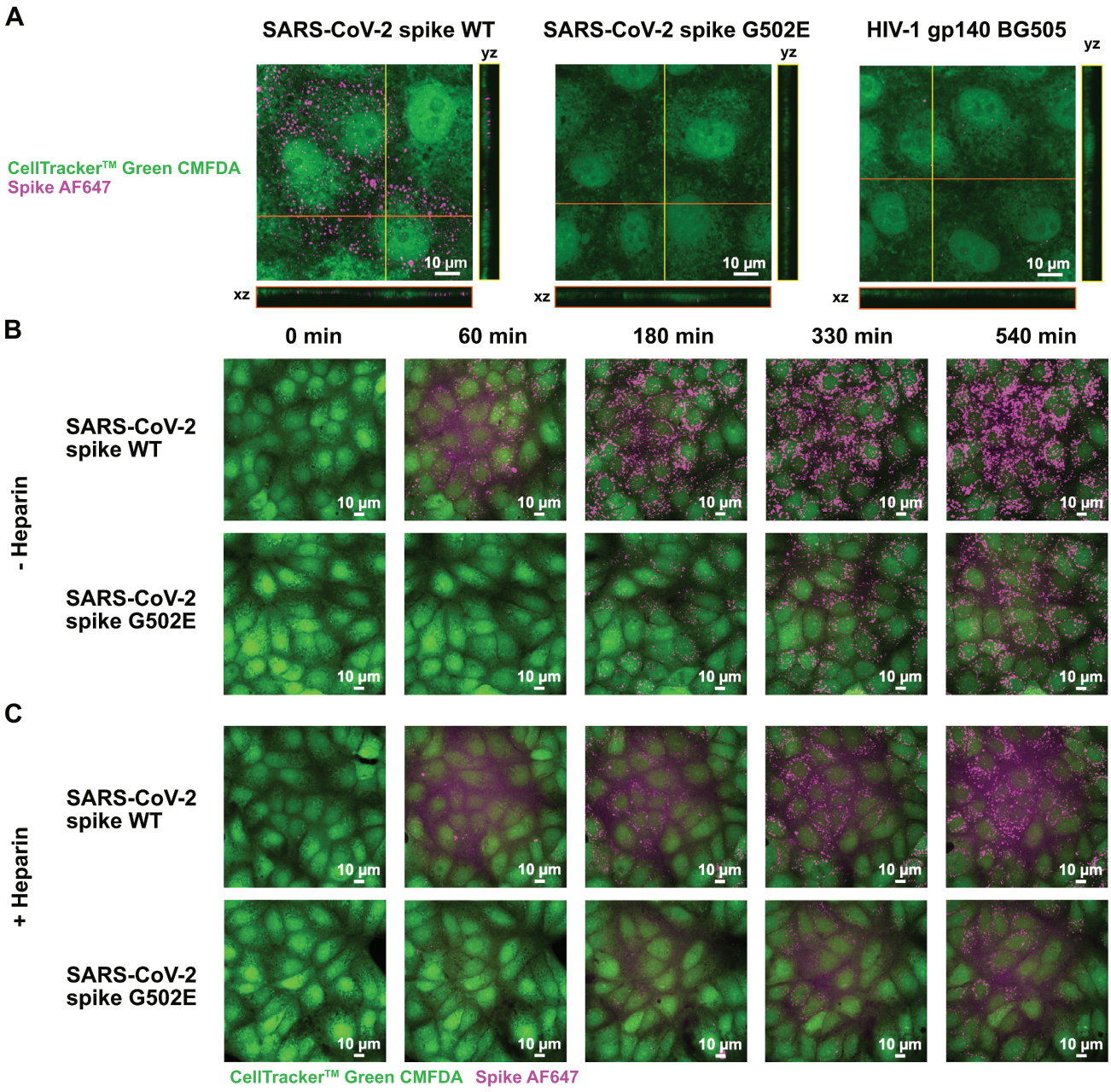

Figure 4. The G502E variant reduces ACE2- but not heparan sulfate-dependent cellular uptake of the SARS-CoV-2 spike. (A) Representative confocal images from two independent experiments showing adsorption of spike WT protein compared with G502E as well as the HIV-1 gp140 BG505 negative control by Vero E6 cells after 90 min of incubation. Shown are z projections with maximum intensity as well as orthogonal views. Scale bars, 10 µm. (B) Live-cell confocal spinning disk microscopy of SARS-CoV-2 spike WT and G502E internalization kinetics was performed in technical duplicates in Vero E6 cells without or (C) with 1 µM Heparin pretreatment over indicated time with representative images as z projections with maximum intensity. For all images, cytoplasm staining with CellTracker™ CMFDA is depicted in green and spike AF647 labeled proteins in magenta. Scale bars = 10 µm. ACE2, angiotensin-converting enzyme 2.

vs WT 1.5-fold increased, $p = 0.2854$; Fig. 6B and Supporting information Fig. S6B). Moreover, we observed a significant improvement of the ACE2 competition potential (BD_{50} G502E vs. WT 2-fold increased, $p = 0.0158$; Fig. 6C and Supporting information Fig. S6C), and neutralization of pseudotyped viral particles (NT_{50} G502E vs. WT 3.3-fold increased, $p = 0.0044$; Fig. 6D). Furthermore, the proportion of class 1 and 2 antibodies, which recognize epitopes including L455, F456, and E484, was significantly improved for G502E over WT (L455R 2-fold increased, $p = 0.0054$; F456A 1.6-fold increased, $p = 0.0978$; E484K 2.4-fold increased, $p = 0.0003$; Fig. 6E). Collectively, our data suggest that the G502E RBD is superior in inducing neutralizing antibody titers compared with other top-scoring candidates such as G502R and Y505G, as well as the RBD WT.

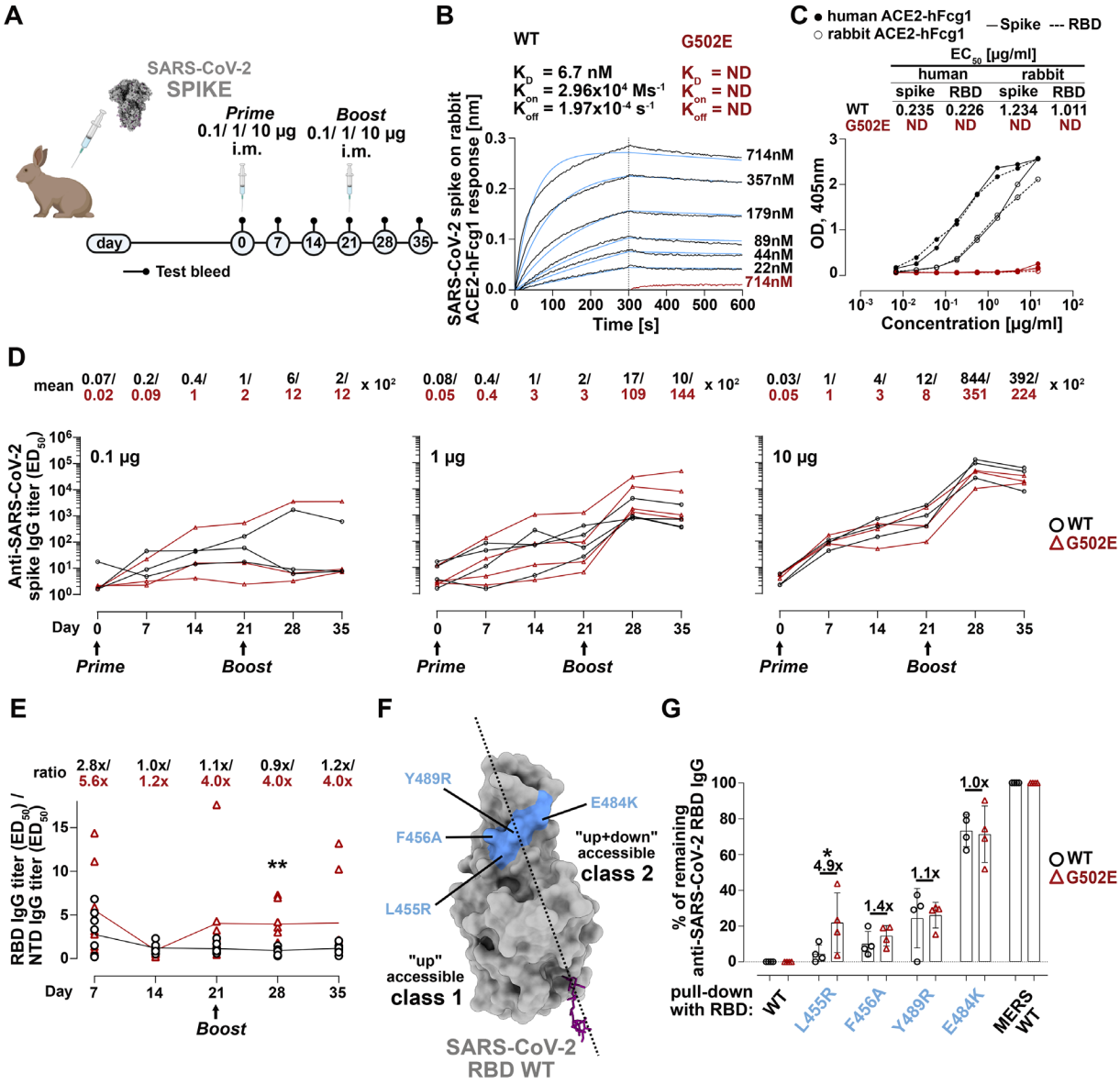

Figure 5. Receptor binding abrogation focuses the antibody response toward the RBD in spike immunizations. (A) Scheme of rabbit immunizations with SARS-CoV-2 spike proteins. i.m., intramuscular. (B) BLI sensorgram shows the binding affinity via dissociation constant (K_D), on-rate (K_{on}), and off-rate (K_{off}) of rabbit ACE2-hFcg1 to SARS-CoV-2 spike WT and G502E. K_D values were calculated using a 1:1 global fitting model and only R^2 values above 0.98 were considered. ND, not detected. (C) ELISA binding of human and rabbit ACE2-hFcg1 fusion proteins to the SARS-CoV-2 RBD and spike WT protein. Optical density curves and the concentration at which 50% of ACE2-hFcg1 is bound (EC_{50}) are shown. ND, not detected. (D) Anti-spike IgG titers (ED_{50}: dilution at which 50% of antibodies are bound) were determined by ELISA for rabbit sera collected from day 0 to 35 upon receiving 0.1 ($n = 3$ rabbits), 1 ($n = 4$ rabbits) and 10 µg ($n = 3$ rabbits) of the immunogen per dose. Mean ED_{50} values are displayed. (E) Ratio of RBD over NTD-specific antibodies was calculated from ED_{50} values of IgG serum reactivity and is displayed on the graph. Four rabbits lacking spike reactive antibodies (2 × WT and 2 × G502E immunized with 0.1 µg per dose) were excluded from the analysis. Two-tailed paired *t*-test was employed. (F) Molecular representation of SARS-CoV-2 RBD WT with class 1 antibody abrogating L455R and F456A, class 1–2 abrogating Y489R as well as class 2 abrogating E484K mutations highlighted in light blue. (G) Rabbit sera were cleared by a pull-down with indicated SARS-CoV-2 variants employing SARS-CoV-2 RBD-WT and MERS-CoV RBD WT as controls. Remaining IgG binding to RBD WT in % and the respective ratio between WT and G502E is displayed. One-tailed unpaired *t*-test was applied. In (D) and (E) mean as a trendline is shown and in (G) mean +/− SD is shown. $^*p = <0.05$; $^{**}p = <0.01$. ACE2, angiotensin-converting enzyme 2; BLI, biolayer interferometry; RBD, receptor binding domain.

Discussion

Taking the SARS-CoV-2 spike as an example, our work introduces the BIBAX antigen design strategy to disable the interaction of vaccines with their host receptors while preserving their immunogenicity. BIBAX aims at overcoming two major obstacles: (1) the negative impacts on host receptor regulatory functions and (2) the limited availabilities of the immunogen through antigen displacement and epitope masking. Through an *in silico* scoring algorithm as well as in vitro and in vivo validations, we identified the

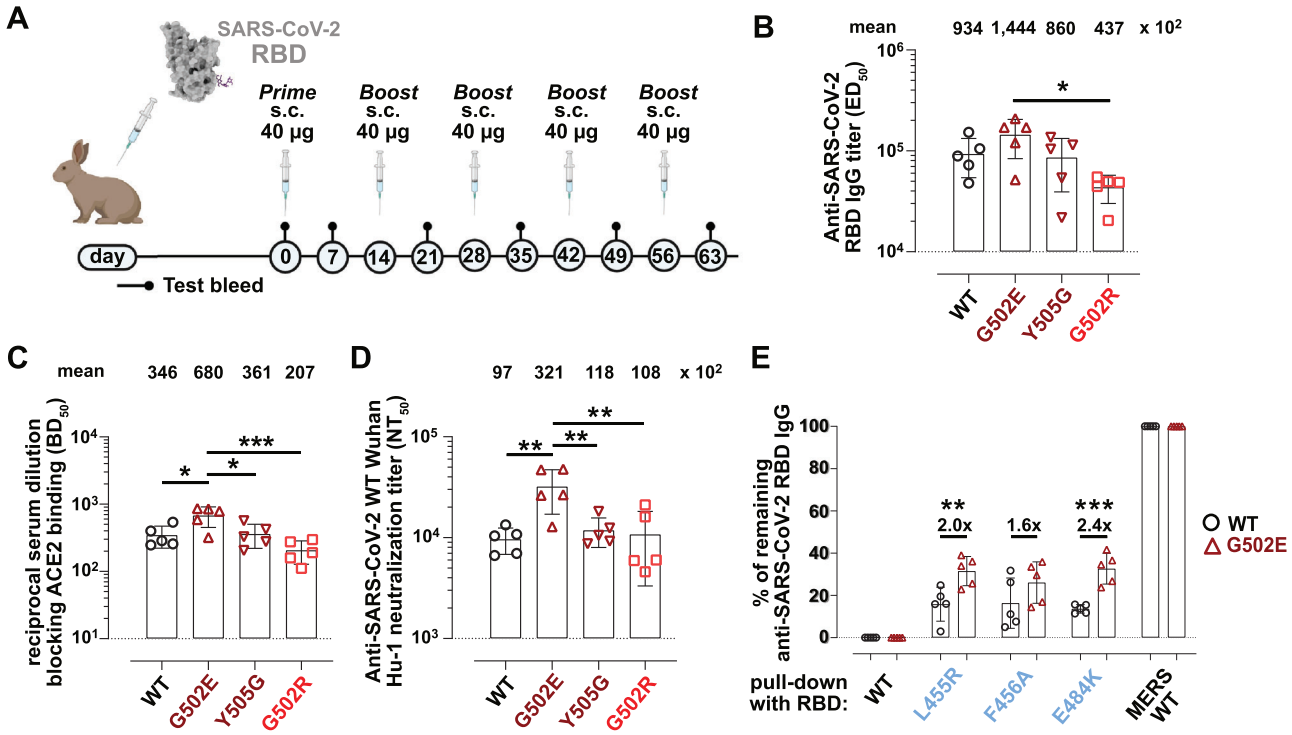

Figure 6. SARS-CoV-2 RBD G502E improves neutralizing antibody titers. (A) Scheme representing the RBD immunization regimen. s.c., subcutaneous. (B) Anti-RBD WT IgG depicted as ED_{50}, (C) reciprocal serum dilution to block 50% of ACE2 binding to the RBD WT (BD_{50}), and (D) neutralization of virus particles pseudotyped (PsV) with SARS-CoV-2 spike WT (NT_{50}) determined at day 35 after prime for animals immunized with recombinant RBD WT, G502E, Y505G, G502R ($n = 5$ rabbits per condition). Samples were subjected to ordinary one-way ANOVA with Tukey's multiple comparison test. (E) Rabbit sera ($n = 5$ rabbits per condition) were depleted via RBD pull-down as shown in Fig. 5F and Supporting information Fig. S4B. One-tailed unpaired *t*-test was applied. In (B–E), mean +/− SD is shown. $^{*}p = <0.05$; $^{**}p = <0.01$; $^{***}p = <0.001$. RBD, receptor binding domain.

G502E variant of the SARS-CoV-2 RBD as the most immunocompetent vaccine candidate, capable of inducing strong neutralizing antibodies but preventing ACE2-dependent cell-to-cell fusion and internalization of the immunogen. In spike immunizations, the G502E exchange focused the immune response toward the RBD, but the overall spike reactive antibody response was similar to WT. When the RBD was used as an antigen, a G502E exchange improved the ACE2 competition potential of serum antibodies as well as the neutralization of pseudotyped virus particles. Nevertheless, increased nAb titers may not directly translate into in vivo protection. While other factors contributing to an improved neutralization of G502E RBDs cannot be entirely excluded at this stage, our data suggest that the abrogation of host receptor binding bears the potential to improve immune responses.

A higher binding affinity of Omicron variants to human and mouse ACE2 compared with WT has been reported [39, 40]. If ACE2 binding would mask the RBM or displace the antigen, Omicron variants would be expected to elicit lower levels of neutralizing antibody titers, which indeed has been reported for protein vaccines [41]. However, the reported effect may also be multifactorial as an extensively altered structural landscape of the RBM may negatively impact immunogenicity and the generation of neutralizing antibodies.

Healthy and diseased human vessels express ACE2 [10, 42]. Furthermore, the ACE2 protein and its enzymatic activity were detected in skeletal muscles [43, 44] and skin tissues [45]. The ACE2 expression pattern would be in agreement with limited antigen or epitope availability following intramuscular or subcutaneous application of a protein-based vaccine. Nevertheless, direct evidence for in vivo displacement of SARS-CoV-2 antigens by endogenous ACE2 demands further studies. Of note, the receptor binding affinity of the SARS-CoV-2 RBD to rabbit ACE2 is only half compared with human, suggesting that the benefit of ACE2 binding abrogation is underestimated in our animal model. Therefore, immunization of transgenic mice expressing hACE2 under the mACE2 promoter [46] may be a preferred model in future studies.

While classical protein-based vaccines have a limited distribution in the body [47], vaccines delivered by novel platforms can be more widely dispersed. For instance, between 20 and 60% of lipid nanoparticles (LNP) or their mRNA content were detected in the liver after intramuscular or intravenous injections [48]. Besides the blood, spleen, and kidney, low amounts of vaccine mRNA were detected in the heart, lung, testis, brain, and eye [49]. Similarly, biodistribution patterns of viral vector vaccines include multiple organs [50]. Given the possibility of dysregulating the receptor function after spreading to various tissues, vaccines lacking host–receptor interaction may be less prone to cause side effects. Certainly, SARS-CoV-2 vaccines show excellent safety profiles and are well tolerated in the vast majority of recipients [51].

Only rarely, severe side effects such as myocarditis and pericarditis were observed and mainly occurred in young healthy males receiving an mRNA vaccine dose [52]. As the risk of myocarditis after COVID-19 vaccination appears similar or even lower compared with traditional vaccines including influenza or smallpox [52], receptor binding may play a minor role. Nevertheless, spike binding may impact ACE2-dependent regulatory systems, which include the renin-angiotensin, the kinin-kallikrein, and the coagulation system [53]. In the future, it needs to be addressed if a lack of receptor interaction has the potential to ameliorate local and systemic dysregulation by avoiding receptor internalization, cellular fusion, or by affecting signaling cascades or enzymatic activities. The evaluation of potential safety benefits, however, usually requires extensive studies with large cohort sizes.

Based on low levels of soluble ACE2 in the blood of healthy individuals [12, 14], masking of SARS-CoV-2 antigens may be rather associated with membranous ACE2. By contrast, other pathogen receptors with high affinity for vaccine antigens occur abundantly in the circulation of healthy individuals, such as the MERS-CoV receptor dipeptidyl peptidase 4 (DPP4) [54]. Therefore, MERS-CoV vaccine antigens may benefit from host receptor-abrogating vaccines. In addition, expansion of the BIBAX design to co-receptors, such as HS, may further support immunogen availability.

Although the use of body-inert vaccines has not been proposed as a general strategy to improve vaccine design thus far, previous reports support the benefits of receptor-abrogating vaccines for certain pathogens. For HIV, a prefusion stabilized HIV glycoprotein that loses CD4 binding was shown to avoid rapid conformational changes and was suggested to prevent the sequestration of antigens by $CD4^+$ expressing T cells [55]. Proof of the latter, however, was hampered by the lack of preclinical animal models that mirror the binding strength of the HIV glycoprotein to human CD4. A meningococcal vaccine, which abrogates binding of the factor H binding protein antigen to serum fH via an R41S single point mutation, significantly improved antibody responses in a human fH transgenic mouse model [7]. However, the R41S variant was less immunogenic in mice lacking human fH [56], underlining the importance to preserve nAb epitopes when optimizing the antigen. For influenza, a very recent report addresses the influence of sialic acid (SA) binding during vaccination, demonstrating that virus-like particles lacking interaction with SA show an improved immunogenicity [57]. Beyond the random selection of receptor-abrogating mutants, the integrated BIBAX strategy provides means to even further improve antibody responses by extending the immunogen design via optimization of expression and recognition by neutralizing antibodies. Finally, it needs to be considered that BIBAX designs may be most beneficial if the receptor-vaccine interaction is of high affinity unless a multimeric antigen platform is applied.

Our work suggests that of all possible single RBD mutations abrogating ACE2 binding, G502E is particularly suited to positively impact humoral immune responses. Except for G502F, all G502 mutations abrogate receptor binding. Therefore, RBD modifications affecting this position are less likely to occur in emerging variants of concern and may be introduced into upcoming vaccine platforms aiming for cross-protective immunity, such as the RBD-based mosaic vaccines [58]. Given that SARS-CoV-2 vaccines may require regular and repeated application to boost the immune response, our work offers a simple modification with the potential to improve vaccine tolerability and antigen availability. Immune escape of viruses and vaccines by host receptor binding has not been systematically studied thus far. Therefore, we provide a methodology that may inform on the general impact of antigen displacement and masking on immune escape during vaccination and may contribute to the improvement of vaccine designs for pathogens lacking preventive measures.

Materials and methods

Cell lines

Vero E6 (ATCC CRL-1586), HEK293T (ATCC CRL-3216), and HEK Flp-In T-REx 293 pFRT/TO/FLAG/HA-ACE2 (kindly provided by E. Wyler, M. Landthaler, and O. Benlasfer) cells were cultured in DMEM / high glucose/GlutaMax™ (Life Technologies; #61965026) + 10% FCS (PAN Biotech; #P30-1902) and 1% Penicillin-Streptomycin (Life Technologies; #15140163) at 37°C and 5% CO_2. Cell lines were not authenticated, but regularly tested for mycoplasma contamination.

Sample donors and cohort characteristics

Samples were obtained from moderate (WHO3-5; $n = 19$) and severe (WHO6-8; $n = 20$) cases of COVID-19. Severity states were categorized according to WHO ordinal scale for clinical improvement: hospitalized mild disease without oxygen therapy (WHO3), hospitalized mild disease with oxygen by mask or nasal prongs (WHO4), hospitalized severe disease with non-invasive ventilation or high-flow oxygen (WHO5), hospitalized severe disease with intubation and mechanical ventilation (WHO6), hospitalized severe disease with intubation, mechanical ventilation, and additional organ support - pressors, RRT, or ECMO (WHO7), death (WHO8). Patients included in this analysis were recruited from March 4, 2020 to January 5, 2021.

The Pa-COVID-19 study cohort was approved by the Charité Ethics Committee (EA2/066/20) and registered at the German Clinical Trials Register and WHO International Clinical Trials Registry Platform (DRKS00021688). The full trial protocol can be accessed at: https://drks.de/search/de/trial/DRKS00021688. The WHO scale for clinical improvement on day 15 was set as the primary outcome and the WHO scale for clinical improvement at discharge from hospital was set as the secondary outcome.

All samples were collected in compliance with the principles laid down in the 1964 Declaration of Helsinki and its later amendments. All patients gave written informed consent.

All 39 patients of this study were hospitalized (WHO3-8) and 74% thereof were male. Female patients had a median age of 60 years (min. 22; max. 82 years) and a median BMI of 29.4 kg/m^2 (min. 24.2; max. 55.6 kg/m^2). Male patients had a median age of 66 years (min. 40; max. 84 years) and a median BMI of 27.4 kg/m^2 (min. 21.3; max. 41.5 kg/m^2). All relevant past diseases data were collected including heart conditions, pulmonary diseases, diabetes, fat metabolism disorders, chronic liver and kidney diseases, and other illnesses.

Collection of sera and plasma

Sera were obtained from blood collected in tubes containing clot activator of silica particles, followed by centrifugation. Plasma was isolated from blood drawn using tubes or syringes prefilled with heparin, followed by 1:2 dilution with PBS/2 mM EDTA and Ficoll density gradient centrifugation. Plasma and sera were stored at 4°C.

Immunization of rabbits

Female New Zealand white rabbits (10 weeks of age) were housed and immunized by Davids Biotechnologie Regensburg. All the procedures were carried out according to German and European Law and were approved by the government of Unterfranken (55.2 2532-2-859). In the RBD immunization setting, five rabbits per condition were vaccinated with 40 μg/mL of SARS-CoV-2 RBD WT, G502E, Y505G, or G502R subcutaneously (s.c.) adjuvanted with AddaVax at a 14-day interval. Test bleeds were taken on day 0, 7, 21, 35, 49, and 63. In the spike immunization setting, rabbits were immunized intramuscularly (i.m.) either with 0.1 μg (three animals/condition), 1 μg (four animals/condition) or 10 μg (three animals/condition) of SARS-CoV-2 spike WT or G502E with Furin cleavage site mutations (682-685 RRAR → QQAQ) [59], the 2P mutation at K986P and V987P for locking the protein in the prefusion conformation [8] as well as four additional Proline mutations to achieve even higher protein stability and yield (HexaPro) [36]. In order to mirror the human administration regimen, rabbits were primed at day 0 and boostered at day 21. Test bleeds were obtained from day 0, 7, 14, 21, 28, and 35. Rabbit sera were subjected to IgG titer determination, ACE2 competition assay and SARS-CoV-2 WT Wuhan Hu-1 pseudovirus (PsV) neutralization analysis, as well as pull-down studies followed by remaining IgG titer determination.

In silico identification of mutant RBDs

In order to identify suitable SARS-CoV-2 vaccine candidates, previously reported deep mutational scanning data of the SARS-CoV-2 RBD complex were used to define a variant feasibility score [20–23] using Python (Python Software Foundation) including libraries pandas [60], numpy [61], matplotlib [62], and Adjust text [63]. The data reflect the impact of all RBD single amino acid substitutions on antigen expression (R_{stab}), escape from binding of neutralizing antibodies (R_{nab}), and reduction of ACE2 receptor binding (R_{endo}). The data were used as selection assays in the original experiments as reported previously [20, 21]. The units of the selection scores are

- R_{stab} – log-ratio of a count, $c(s)$, for a sequence s and a count of a reference antigen, $c(r)$. Expression: $R_{\text{stab}} = \log c(s)/c(r)$
- R_{nab} – escape fraction specifying a count with decreased binding compared with a total count.
- R_{endo} – log-ratio of a dissociation constant, $K(s)$, of a sequence, s, to a dissociation constant of a reference antigen, r. Expression: $\log K(s)/K(r)$

For preprocessing and standardization, we selected data based on two constraints: R_{stab} of variant should be at least a factor of $\exp(-\alpha)$ of the reference and R_{endo} of variant should be at most a factor of $\exp(-\beta)$ of the reference. We used $\alpha = 0.5$ and $\beta = 1.0$ corresponding to considering mildly destabilized (>60%) and low binding variants (>36%).

After selecting the variants which fulfill the constraints outlined above, we computed the normalized fitness score by first subtracting the sample mean fitness and then dividing by the sample standard deviation. We refer to the corresponding normalized scores as $\mathrm{N}_{\text{stab}}(s)$, $\mathrm{N}_{\text{nab}}(s)$, and $\mathrm{N}_{\text{endo}}(s)$. At this stage, all missing scores – e.g. values not reported in ref – were imputed to 0 (the average under the normalization).

For score computation, we summarized the normalized scores to a total feasibility score of a variant compared with the reference, to help identify possible candidate variants to test experimentally:

$$\mathrm{S}_{\text{tot}}(s) = N_{stab}(s) - N_{nab}(s) - N_{endo}(s),$$

which was larger for better (more feasible) variants s. We subselected variants in the primary (residues 443–463 and 469–507) and secondary (residues 403–410 and 417–423) interface region defined using previously reported complex structures (PDB: 6XC2, 6XCN, 6XDG, 6XE1, 6XKQ, 7CDI, 7CDJ, 7JMO, 7JMP, 7JMW, 7JV2, 7JV6, 7JVA, 7JW0, 7K90, 7LX5). Following the subselection, we sorted all remaining variants according to S_{tot}.

For the identification of interaction hotspots and selection of variants, we categorized hotspots by sorting the loci by their highest-scoring variant. Negative scoring loci were discarded. A threshold, γ (range from 0 to 1), represented the fraction of non-negative maximum total-scoring loci to exclude, larger as more specific but fewer hits. We used $\gamma = 0.40$. We suggest first taking the highest-ranked variant from each locus and then exploiting and investigating, respectively, lower-ranked variants for each locus in subsequent libraries.

Cloning of recombinant glycoproteins and antibodies

SARS-CoV-2 RBD WT was cloned containing the signal peptide spanning amino acids M1-Q14 and R319-F541 of the pCAGGS-SARS-CoV-2 RBD Wuhan plasmid [64] (kindly provided by F. Krammer; GenBank: MN908947.3), followed by a C-terminal Twin-Strep-tag sequence (WSHPQFEKGGGSGGGSGGSAWSHPQFEK) and a hexahistidine tag. SARS-CoV-2 spike encoding plasmid comprised the amino acids M1-Q1208 of the Wuhan SARS-CoV-2 variant (GenBank: MN908947.3) with Furin cleavage site mutations (682- 685 RRAR → QQAQ) [59] as well as 6 Proline mutations (HexaPro) to generate a protease-resistant, stable, and highly immunogenic SARS-CoV-2 spike protein locked in the prefusion conformation [36, 65] followed by a TEV protease site (RENLYFQG), a foldon trimerization motif (YIPEAPRDGQAYVRKDGEWVLLSTFL) as well as a Twin-Strep-tag and a hexahistidine tag. For expression of the membrane-bound version, a SARS-CoV-2 spike full-length vector with a C-terminal 19 amino acid deletion [66] comprising amino acids M1-C1254 of the Wuhan SARS-CoV-2 variant (GenBank: MN908947.3) was used. Mutations of RBD and full spike were introduced by PCR mutagenesis to create the determined in silico candidates. The N-terminal domain (amino acids M1-S305) of the SARS-CoV-2 spike was cloned to a C-terminal Twin-Strep-tag and a hexahistidine tag. The signal peptide of SARS-CoV-2 (M1-Q14) was linked to an Avi-tag (GLNDIFEAQKIEWHE) followed by MERS-CoV RBD WT [67] (G372-L588) and C-terminal Twin-Strep-tag as well as hexahistidine tag. The HIV-1 gp140 protein is based on the BG505 isolate sequence (GenBank: DQ208458), but modified with flexible peptide covalent linkages between gp120 and gp41 subdomains (BG505 NFL) instead of a furin cleavage site to yield soluble, native-like trimers [68]. Plasmids containing human full-length ACE2 (Clone: OHu20260C; M1-F805) and rabbit full-length ACE2 (Clone: OOb21562C; M1-F805) C-terminally linked to enhanced green fluorescent protein (eGFP) were purchased from Genscript (GenScript Biotech Netherlands B.V.). Heavy and light chain sequences of neutralizing antibodies were cloned into IgG1 heavy and kappa or lambda light chain expression vectors from Oxgene (Sigma-Aldrich; #PP2409-1KT): class 1–4 anti-SARS-CoV-2 RBD: EY6A [69], P2B-2F6 and P2C-1F11 [70], REGN10933 and REGN10987 [26], CC12.1 [28], C144 [27], S2H13 [17], S309 [71], anti-SARS-CoV-2 NTD: 4A8 [72], anti-MERS-CoV: LCA60 [73], anti-HIV-1: VRC01 [74]. Human ACE2-hFcg1 was produced by fusing recombinant human ACE2 Q18-V739 fragment to human IgG1-Fc (E99-K330 portion, where the first amino acid is G encoded by J-CH1 fusion) [75]. Similarly, rabbit ACE2-hFcg1 was produced recombinantly by fusing rabbit ACE2 Q18-P740 fragment to human IgG1-Fc.

Production of recombinant proteins

Cloning constructs were used to transiently transfect FreeStyle™ 293-F cells (Life Technologies; #R79007) that were grown in suspension using Expi293™ expression medium (Life Technologies; #A1435101) at 37°C in a humidified 8% CO_2 incubator shaking at 125 rpm. Cells were grown to a density of 2.5 million cells per mL, transfected using polyethylenimine (PEI; Polysciences Europe GmbH; #23966-1; 4 μg/mL in cell suspension) and plasmid DNA (1.2 μg/mL in cell suspension) that were diluted in Opti-MEM™ (Gibco; #31985047) medium, and cultivated for 3 days. The supernatants were harvested and proteins purified by His or Ab SpinTrap columns according to the manufacturer's protocol (Cytiva; His: #28-9321-71; Ab: #28-4083-47). The eluted protein was buffer exchanged to PBS (Sigma-Aldrich; #D8537-500ML) using Amicon Ultra-4 ultrafiltration column with 10 kDa (Millipore, #UFC801096) or 100 kDa cutoff (Millipore, #UFC810008). Protein concentration was determined by Nanodrop. Protein production was confirmed by Western Blot.

Biolayer interferometry

To determine the binding affinity of SARS-CoV-2 spike variants to the ACE2 receptor, human and rabbit ACE2-hFcg1 were loaded at 20 μg/mL in 1 x kinetics buffer (Sartorius; #18-1105) onto a Protein A biosensor (Sartorius; #18-5010) for 600 sec. Following a baseline step for 120 s, SARS-CoV-2 spike variants were added at 714 nM starting concentration and subsequent two-fold dilutions for 300 s to determine the association rate, ensued by dipping the sensor into the kinetics buffer for another 300 s for measuring the dissociation rate. After every cycle, sensors were regenerated every 5 s by alternating 10 mM Glycine pH 1.5 buffer (Roth GmbH; #3790.2; regeneration) and 1 × kinetics buffer (neutralization). All steps were performed at 1000 rpm shaking speed and room temperature. Data were acquired with an Octet® R4 BLI Discovery system, analyzed with Octet® Analysis Studio software v12, and curves depicted via GraphPad Prism 8.1.2 (GraphPad Software Inc.). K_D values were calculated using a 1:1 global fitting model and only R^2 values above 0.98 were considered.

RBD pull-downs

Antibody depletion of sera from COVID-19 patients was performed with SARS-CoV-2 RBD WT, MERS-CoV RBD WT, or mutant RBDs (from high to low score: G502E, Y505G, G502R, L455R, Y489R, E484K) to determine the strength of antibody retention for each variant. To evaluate the amount of ACE2 competing class 1–2 antibodies, pull-downs from sera of immunized rabbits were conducted with SARS-CoV-2 RBD WT and MERS-CoV RBD WT control proteins as well as mutant RBDs that abrogate the majority of class 1 neutralizing antibodies (L455R, F456A), class 1–2 neutralizing antibodies (Y489R), and class 2 neutralizing antibodies (E484K). Upon equilibration according to the manufacturer´s protocol, 120 μL of 5% Strep-Tactin® XT magnetic beads (IBA GmbH, #2-4090-002 or -010) were coupled with 24 μg of recombinant RBD via the C-terminal Twin-Strep-tag at 37°C for 1 h. The unbound RBD was removed by pelleting the magnetic beads

and the latter were washed three times in 1 mL PBS. Beads were blocked with PBS/1% BSA (Thermo Fisher; #30063572) shaking at 37°C for 1 h. After another washing, serum was added to the beads to reach a final dilution of 1:10 in 200 μL final volume and incubated in a rotisserie shaker overnight at 4°C. The next day, tubes were placed on a magnetic holder and supernatants were collected. Binding and neutralization potential of the remaining antibodies was analyzed via antigen-specific IgG ELISA, ACE2 competition ELISA and PsV neutralization assay. Percentages of remaining antibodies after depletion with mutant RBDs were determined by dividing calculated logarithmic area under curve values of each sample by the respective S309 antibody standard followed by normalization of samples with MERS-CoV WT (negative control; corresponding to 100%) and SARS-CoV-2 WT (positive control; corresponding to 0%) RBD pull-downs.

ELISA to determine antigen-specific IgG

Recombinantly expressed SARS-CoV-2 S1 RBD, NTD, or S1+S2 spike protein was coated on a high-binding 96-well ELISA plate (Corning, #CLS3690) at 10 μg/mL diluted in PBS overnight at 4°C. Plates were blocked for 1 h with PBS/1% BSA at room temperature. Sera and proteins were serially diluted in PBS/1% BSA, added to coated plates and incubated for 1 h at room temperature. Plates were developed with an anti-human IgG-alkaline phosphatase (AP)-coupled antibody (Southern Biotech, #2040-04) or anti-rabbit IgG-AP conjugated antibody (Jackson ImmunoResearch; #111-056-003) both diluted 1:500 in PBS/1% BSA. Bicarbonate buffer containing 4-nitrophenyl phosphate disodium salt hexahydrate substrate (Sigma, #S0942-50TAB) was added and absorbance was measured at 405 nm in a Cytation 5 device (Agilent BioTek). Between all indicated incubation steps, plates were washed three times with PBS / 0.05% Tween-20. IgG titers (ED_{50}) were determined via sigmoid curve fitting with non-linear regression performed in R (stats package) and further normalized by calculating the ratio between the ED_{50} of the sample and the ED_{50} of the reference antibody on the same ELISA plate. For curve fitting, upper and lower plateaus of the S309 (RBD) or 4A8 (NTD) reference antibodies were applied to all respective samples.

ACE2 competition ELISA (surrogate virus neutralization assay)

Upon 1 h blocking with PBS/1% BSA, serially diluted sera in PBS/1% BSA were added to SARS-CoV-2 RBD-coated (10 μg/mL) 96 well plates. After 1 h of incubation at room temperature, self-produced biotinylated human ACE2-hFcg1 was added to a 70% final effective concentration (EC_{70}) in PBS / 1% BSA for competition with serum antibodies. After another hour at room temperature, plates were incubated with an AP-coupled streptavidin (Southern Biotech, #SBA-7105-04) at a 1:500 dilution in PBS/1% BSA to detect biotinylated ACE2-hFcg1 that was not prevented by serum antibodies from binding to RBD. The 50% blocking dose (BD_{50}) was determined by sigmoid curve fitting with non-linear regression performed in R (stats package). Upper and lower plateaus of the (non-)biotinylated ACE2-hFcg1 control served as a reference.

Production and titration of SARS-CoV-2 pseudoviruses (PsV)

HEK293T cells were transfected with plasmids containing a Luciferase reporter, lentiviral structure proteins (gag/pol) as well as codon-optimized SARS-CoV-2 full-length spike WT Wuhan Hu-1 containing a cytoplasmic 19 amino acid truncation. One day posttransfection, the medium was exchanged and cells incubated for another 24 h in a 5% CO_2 environment at 37°C. After 48 and 72 h of transfection, the medium containing the lentiviral pseudoparticles was harvested by passing through 0.45 μM filter units and equally separated into polypropylene tubes (Beckman Coulter, #326823). Samples were centrifuged in a Beckman Coulter L-60 ultracentrifuge with an SW 32 Ti rotor at 24,000 rpm for 90 min at 4°C and thereafter supernatant was discarded. The virus-containing pellet was reconstituted with 1 x Hank's balanced salt solution (Gibco; #14025092), aliquoted, and stored at −80°C for subsequent titration and neutralization assays, respectively.

Titration was carried out in hexaplicates with a three-fold dilution series, in which the last column serves as a negative control as outlined in Nie et al. [76]. 12.5×10^4 HEK Flp-In T-REx 293 pFRT/TO/FLAG/HA-ACE2 cells were seeded in a 96 well plate and incubated 1:1 (v/v) with the respective PsV dilution on the next day. After 48 h of incubation, medium was taken off and Bright-Glo™ Luciferase substrate (Promega; #E2620) was added 1:1 (v/v) to the cells. The suspension was then transferred to white 96 well plates (Corning, #3688) and after 5 min luminescence was measured in a Cytation 5 device. The 50% tissue culture infectious dose ($TCID_{50}$) was determined based on the Reed-Muench method as described previously [76, 77].

SARS-CoV-2 PsV neutralization assay

12.5×10^4 HEK Flp-In T-REx 293 pFRT/TO/FLAG/HA-ACE2 cells were seeded in 96 well plates. The next day ACE2-hFcg1 as the standard (diluted to 20 μg/mL start concentration, followed by four-fold serial dilutions), or remaining antibodies in pull-down fractions from human sera (diluted to 1:10 start, followed by three-fold dilutions), or rabbit sera (diluted to 1:50 start, followed by five-fold dilutions) were mixed 1:1 (v/v) with 1300–2600 $TCID_{50}$ of SARS-CoV-2 WT Wuhan Hu-1 PsV and incubated 1 h at 37°C. Then the virus-antibody mixture was transferred on top of cells at a ratio of 1:1 (v/v) and incubated for further 48 h at 37°C. After incubation, medium was taken off and Bright-Glo™ Luciferase substrate was added 1:1 (v/v) to the cells. The suspension was then transferred to white 96 well plates and after

5 min luminescence was measured in a Cytation 5 device. The 50% neutralizing titer (NT_{50}) was determined using non-linear regression in GraphPad Prism based on sigmoid curve analysis, using the human ACE2-hFcg1 curve as a standard on every plate.

Flow cytometry

All fluorescently labeled proteins used in this study were generated using the Alexa Fluor® 647 (AF647) antibody labeling kit from Thermo Fisher according to the manufacturer's instructions (Thermo Fisher, Life Technologies, #A20186). To determine the binding of SARS-CoV-2 RBD proteins to ACE2 on Vero E6 and HEK Flp-In T-REx 293 pFRT/TO/FLAG/HA-ACE2 cell lines, 200,000 cells were stained with 10 μg/mL of AF647-conjugated RBD variants for 20 min at 4°C. Cells were washed in FACS buffer (PBS + 10% FCS + 2mM EDTA) containing DAPI (1:1500; BD Biosciences, #564907) for 5 min at 350 x *g* and resuspended in FACS buffer for flow cytometry analysis.

40,000 Vero E6 cells were seeded in a 24-well plate and PEI transfected with 0.8 μg of selected in silico determined SARS-CoV-2 full-length mutants. After 20–24 h, cells were trypsinized and stained with 30 μg/mL anti-SARS-CoV-2 nAb S309 for 20 min at 4°C. Upon washing with FACS buffer containing DAPI (1:1500), goat anti-human IgG AF647 (Jackson ImmunoResearch, #109-606-170) at a dilution of 1:500 was used as secondary antibody for detection of SARS-CoV-2 full-length spike expression on cells.

A total of 10,000 events were acquired on a BD LSRFortessa™ device. Cells were first gated by FSC-A and SSC-A and subsequent SSC-A and DAPI gating to exclude dead cells. The viable population was checked for AF647 expression and data was analyzed via FlowJo v10.8.1 software.

Western blotting

To confirm protein production and concentration, recombinantly expressed SARS-CoV-2 RBD and spike proteins were loaded to a 4–15% Mini-PROTEAN® TGX Stain-Free™ Protein polyacrylamide gel (Bio-Rad, #4568083) together with the Precision Plus Protein Dual Color Standard (Bio-Rad, #1610374). Subsequently, proteins were transferred to a Trans-Blot Turbo Midi 0.2 μm Nitrocellulose membrane (BioRad, #1704159), blocked with 30 mL of 5% skimmed cow milk diluted in trisaminomethane-buffered saline with 0.1% Tween-20 (TBST) for 1 h at room temperature on the orbital shaker. The membrane was stained in 5 mL containing mouse anti-hexahistidine antibody (Abcam, #ab18184) diluted 1:1000 at 4°C overnight with constant mixing on the roller. The stained membrane was washed five times with 30 mL of TBST and stained with IRDye® 800CW donkey anti-mouse IgG (LI-COR Bioscience, #925-32212) antibodies diluted 1:5000 for 1 h at room temperature with constant mixing on the roller. The membrane was washed three times with 30 mL TBST and scanned with an infrared membrane scanner (LI-COR Odyssey IR scanner). The protein concentration was determined by densitometry analysis with GelAnalyzer 19.1 (http://www.gelanalyzer.com/ by Istvan Lazar Jr., PhD and Istvan Lazar Sr., PhD, CSc) comparing protein intensities with each other or to the intensity of 200, 100, and 50 ng of recombinant SARS-CoV-2 S1+S2 ECD His standard protein (Sino Biological Europe; #SIN-40589-V08B1-100).

Confocal fluorescence microscopy

To visualize the internalization of the SARS-CoV-2 spike and RBD proteins, 40,000 Vero E6 cells were seeded in wells of an eight-well Ibidi glass bottom slide (Ibidi; #80827). The next day, cells were washed once in PBS and nuclei were stained with NucBlue™ LIVE/READY™ Hoechst 33342 Reagent (Life Technologies, #R37605) according to the manufacturer's instructions for 15 min at 37°C. After another PBS wash, cells were stained with prewarmed CellTracker™ Green CMFDA solution (Invitrogen, #C2925; working concentration: 8 μM) and incubated for 30 min at 37°C. Thereafter, the CMFDA solution was taken off, and free dye was quenched by the addition of FCS containing medium for 5 min. Upon another PBS wash, cells were treated with 10 μg/mL RBD solution or 20 μg/mL spike solution of SARS-CoV-2, as well as SARS-CoV-2 NTD or HIV-1 gp140 BG505 isolate control proteins, respectively. After incubation for 90 min at 37°C, cells were washed once with PBS and fixed with 4% PFA + 20% sucrose in PBS for 20 min at 4°C. Thereafter, cells were washed and kept in PBS. Images of fixed samples were acquired on a Zeiss Laser Scanning confocal microscope (LSM780). For the detection, a photomultiplier was used. The system was controlled by the Zeiss ZEN2010 software (Carl Zeiss Microscopy). Single- and multi-color confocal imaging of fixed samples was performed in sequential mode with the following fluorophore-specific excitation (Ex.) and emission filter (EmF.) settings: Hoechst (Ex.: 405 nm; EmF.: 415–480 nm), CMFDA (Ex.: 488 nm; EmF.: 490–578 nm), AF647 (Ex.: 633 nm; EmF.: 638–735 nm). Images were acquired with a PL APO DIC M27 63x/1.40 NA oil objective (Carl Zeiss Microscopy). A z-stack from bottom to top of the cells was performed over 8 μm with 0.39 μm intervals. Contrast adjustment, z-projection, and orthogonal views were performed using FIJI software (https://imagej.net/software/fiji/). Each condition was performed in duplicates.

Live-cell imaging of RBD and spike protein absorption was performed by incubating Vero E6 cells with prewarmed CellTracker™ Green CMFDA solution (working concentration: 8 μM) for 30 min at 37°C. Thereafter, the CMFDA solution was taken off, and free dye was quenched by the addition of FCS containing medium for 5 min. Upon a PBS wash, cells were either pretreated with 1 μM porcine heparin (Sigma-Aldrich; #H3393-50KU) or medium only for 1 h. Cells were imaged in live-cell imaging buffer Fluorobrite DMEM medium (Gibco, #A1896701) + 10% FCS and 1% Penicillin-Streptomycin. SARS-CoV-2 spike WT and G502E solutions were added to the respective wells to a final concentration of 20 μg/mL. SARS-CoV-2 RBD WT and G502E were added to a final concentration of 10 μg/mL. Dual-color live-cell imaging

was performed with a Nikon Spinning Disk Confocal Microscope equipped with a Nikon TiE with Perfect Focus System, Yokogawa CSU-X-1, automatic stage, and heatable humidity chamber. The system was controlled by the Nikon NIS Elements software (NIS 5.02.01 (Build 1270)). Cells were imaged at 37°C and 5% CO_2 controlled by an OKOLAB system. For image acquisition, a 40 × NA 0.95 air objective and for detection an EMCCD camera (Andor AU-888) were used. The images were acquired in a 16-bit format, with 1024 × 1024 pixels and a total size of 163 × 163 μm. The cell stain CMFDA was excited with a 488 nm laser (150 mW) and AF647 labeled proteins with a 640 nm laser (100 mW). The laser power and the exposure time were kept the same throughout one experiment. For each well of a μ-Slideeight-well Ibidi glass bottom chamber five different positions were imaged. A z-stack (11 slices, 0.6 μm step size) was set for every position using the Nikon Ti Z-Drive. For the time-lapse the first image (0 min) was taken before addition of the labeled protein, the second image right after the addition, and then continuously every 30 min for at least 9 h. Contrast adjustment, z-projection, and time point selection were performed using FIJI. Selected time points of the differently treated wells are shown. Triplicates of each condition were performed.

Vero E6 syncytia formation and HEK293T cell-cell fusion assay

To determine fusogenic potential of in silico-determined SARS-CoV-2 variants, Vero E6 cells were transfected using PEI in triplicates with different SARS-CoV-2 spike full-length proteins together with a pMAX-GFP reporter plasmid (GFP from *P. plumata*; kind gift from A. Lanzavecchia) at a 1:1 ratio. SARS-CoV-1 full-length spike protein served as a control. After 48 h, cells were stained with NucBlue™ LIVE/READY™ Hoechst 33342 Reagent and imaged using Phase contrast, DAPI, and GFP channels/filters of a Cytation 5 device to observe syncytia formation. Pictures taken at 10 × magnification were used for image display as well as syncytia and nuclei count via ImageJ. Each replicate was counted three times and the average was taken.

HEK293T cells were seeded in duplicates and separated into two groups – the donor group was PEI transfected with different SARS-CoV-2 full-length spike proteins as well as the SARS-CoV-1 full-length spike control protein; the acceptor group was PEI transfected with the human ACE2-eGFP plasmid. The next day cells of both groups were mixed with each other at a ratio of 1:1 and seeded in a 24-well plate. After 24 h, cells were treated and analyzed as described for Vero E6 cells.

Scheme visualization and protein structure analysis

Schemes were generated using the software BioRender.com. Protein structure models and molecular analyses were performed with UCSF Chimera X 1.3 [78] using the following PDB codes: 6XDG for SARS-CoV-2 RBD WT and REGN10933 IgG [26], 6XC2 for CC12.1 IgG [79], 7CDI for P2C-1F11 IgG [25], 6M0J for human ACE2 [80], 1HZH for a human IgG1 antibody [81], as well as 6WPS and 7KJ5 for SARS-CoV-2 spike WT [71, 82].

Data presentation and statistical analysis

Figure panels were generated using Affinity Designer software (Serif Europe Ltd., UK). Shown experiments involved minimum $n = 3$ biological replicates (unless otherwise indicated) and produced comparable results. Images obtained in syncytia and cell–cell fusion assays as well as confocal microscopy images were processed with Fiji and ImageJ, respectively. Data from ELISA, syncytia formation, and PsV neutralization assays were analyzed using R 4.0.3, RStudio 1.2.5001, and GraphPad Prism 8.1.2 software. Statistical tests were one- or two-tailed, and a p value lower than 0.05 was considered statistically significant. A Shapiro–Wilk test was used to determine the normality of the distribution for continuous variables. Unpaired/paired t-tests or ordinary one-way ANOVA with Tukey's multiple comparison test of means was used if continuous data met the criteria of the normality test. Otherwise, unpaired Mann–Whitney test was employed. The median or mean (+/− SD if applicable) is shown.

Acknowledgements: The German Research Foundation (394523286, to K.D.L.R.); the Helmholtz association (to K.D.L.R.); Berlin Institute of Health & Stiftung Charité (to K.D.L.R); The European Research Council grant (948464 "Auto-Engineering"; to K.D.L.R); The Helmholtz Association's Initiative and Networking Fund (Project "Virological and immunological determinants of COVID-19 pathogenesis – lessons to get prepared for future pandemics"; KA1-Co-02 "COVIPA", to K.D.L.R.); German Federal Ministry of Education and Research (NaFoUniMedCovid19 – COVIM, NAPKON, FKZ: 01KX2021, PROVID - FKZ 01KI20160A, Pa-COVID-19 Study; to L.E.S., F.K.). This work was partially supported by the Wallenberg AI, Autonomous Systems and Software Program (WASP) funded by the Knut and Alice Wallenberg Foundation (to S.O.). We thank the Pa-COVID-19 Study Group, especially Charlotte Thibeault, Denise Treue, Tatjana Schwarz, and Jan-Moritz Döhn for sample collection, testing, and biobanking. We thank Florian Krammer for providing the SARS-CoV-2 RBD expression plasmid. We thank Anja Schütz and the MDC protein production facility for supporting large-scale purifications of recombinant proteins. Thank you to Hans-Peter Rahn and Kirstin Rautenberg from the MDC flow cytometry core facility Berlin-Buch. We thank Christiane Schüler and Christine Goffinet for providing Luciferase reporter and lentiviral packaging plasmids enabling PsV production. HEK Flp-In T-REx 293 pFRT/TO/FLAG/HA-ACE2 cells were generously provided by Emanuel Wyler, Markus Landthaler, and Ouidad Benlasfer. A big

thank you to Julia Christine Gutjahr for her valuable scientific input and discussion.
Open access funding enabled and organized by Projekt DEAL.

Author contributions: C.R. and K.D.L.R. designed the experiments. L.S., A.uW.A., C.V.G., C.S., and C.R. established and performed immuno-assay and binding studies. C.G., L.S., Mi.L., and C.R. cloned, sequenced, and expressed recombinant proteins. C.R. and H.G. performed microscopy experiments. H.G. and Ma.L. discussed microscopy experiments. L.E.S. and F.K. provided patient samples and clinical data. S.O. established and performed in silico analysis. Mi.L., C.V.G., C.R., and K.D.L.R. analyzed the data. C.R. and K.D.L.R reviewed and edited the draft. C.R. contributed to the original draft. K.D.L.R. acquired funding, analyzed data, wrote the original draft, and supervised and conceptualized the work. All authors read and approved the manuscript.

Conflict of interest: The Max Delbrück Center for Molecular Medicine (MDC) and the Berlin Institute of Health at Charité (BIH) have filed three patent applications in connection with this work on which Mi.L., F.K., L.E.S., and K.D.L.R. (EP21155584.2); C.R., Mi.L., C.V.G, C.S., S.O., and K.D.L.R. (EP21194414.5); C.V.G, C.S., S.O., and K.D.L.R. (EP22164013.9) are inventors. "BIBAX" was registered as a trademark in EU and non-EU countries.

Data availability statement: The code generated for in silico identification of vaccine candidates (Fig. 1) is openly available in the GitHub repository at https://github.com/olsson-group/bibax.

References

1 **Pollard, A. J. and Bijker, E. M.**, A guide to vaccinology: from basic principles to new developments. *Nat. Rev. Immunol.* 2021; **21**: 83–100.

2 **Henry, C. and Jerne, N. K.**, Competition of 19S and 7S antigen receptors in the regulation of the primary immune response. *J. Exp. Med.* 1968. **128**: 133–152.

3 **Reth, M., Kelsoe, G. and Rajewsky, K.**, Idiotypic regulation by isologous monoclonal anti-idiotope antibodies. *Nature*. 1981. **290**: 257–259.

4 **Xu, H. and Heyman, B.**, IgG-mediated suppression of antibody responses: Hiding or snatching epitopes? *Scand. J. Immunol.* 2020. **92**: e12921.

5 **Meyer-Hermann, M.**, Injection of antibodies against immunodominant epitopes tunes germinal centers to generate broadly neutralizing antibodies. *Cell Rep.* 2019. **29**: 1066–1073.e5. Available at: https://www.sciencedirect.com/science/article/pii/S2211124719312550

6 **Principato, S., Pizza, M. and Rappuoli, R.**, Meningococcal factor H binding protein as immune evasion factor and vaccine antigen. *FEBS Lett.* 2020. **594**: 2657–2669.

7 **Isabella, C., Rolando, P. and Granoff, D. M.**, Human factor H (FH) impairs protective meningococcal anti-FHbp antibody responses and the antibodies enhance FH binding. *mBio*. 2014. **5**: e01625–14.

8 **Wrapp, D., Wang, N., Corbett, K. S., Goldsmith, J. A., Hsieh, C.-L., Abiona, O., Graham, B. S. et al.**, Cryo-EM structure of the 2019-nCoV spike in the prefusion conformation. *Science*. 2020. **367**: 1260–1263.

9 **Donoghue, M., Hsieh, F., Baronas, E., Godbout, K., Gosselin, M., Stagliano, N., Donovan, M. et al.**, A novel angiotensin-converting enzyme–related carboxypeptidase (ACE2) converts angiotensin I to angiotensin 1–9. *Circ. Res.* 2000. **87**: E1–E9.

10 **Hikmet, F., Méar, L., Edvinsson, Å., Micke, P., Uhlén, M. and Lindskog, C.**, The protein expression profile of ACE2 in human tissues. *Mol. Syst. Biol.* 2020. **16**: e9610.

11 **Lambert, D. W., Yarski, M., Warner, F. J., Thornhill, P., Parkin, E. T., Smith, A. I., Hooper, N. M. et al.**, Tumor necrosis factor-alpha convertase (ADAM17) mediates regulated ectodomain shedding of the severe-acute respiratory syndrome-coronavirus (SARS-CoV) receptor, angiotensin-converting enzyme-2 (ACE2). *J. Biol. Chem.* 2005. **280**: 30113–30119.

12 **Patel, S. K., Juno, J. A., Lee, W. S., Wragg, K. M., Hogarth, P. M., Kent, S. J. and Burrell, L. M.**, Plasma ACE2 activity is persistently elevated following SARS-CoV-2 infection: implications for COVID-19 pathogenesis and consequences. *Eur. Respir. J.* 2021. **57**: 2003730. Available at: http://erj.ersjournals.com/content/57/5/2003730.abstract

13 **Kragstrup, T. W., Singh, H. S., Grundberg, I., Nielsen, A. L.-L., Rivellese, F., Mehta, A., Goldberg, M. B. et al.**, Plasma ACE2 predicts outcome of COVID-19 in hospitalized patients. *PLoS One*. 2021. **16**: e0252799.

14 **van Lier, D., Kox, M., Santos, K., van der Hoeven, H., Pillay, J. and Pickkers, P.**, Increased blood angiotensin converting enzyme 2 activity in critically ill COVID-19 patients. *Erj. Open Res.* 2021. **7**: 00848–02020. Available at: http://openres.ersjournals.com/content/7/1/00848-2020.abstract

15 **Reindl-Schwaighofer, R., Hödlmoser, S., Eskandary, F., Poglitsch, M., Bonderman, D., Strassl, R., Aberle, J. H. et al.**, ACE2 Elevation in Severe COVID-19. *Am. J. Resp. Crit. Care*. 2021. **203**: 1191–1196.

16 **Rahman, M. M., Hasan, M. and Ahmed, A.**, Potential detrimental role of soluble ACE2 in severe COVID-19 comorbid patients. *Rev. Med. Virol.* 2021. **31**: e2213.

17 **Piccoli, L., Park, Y.-J., Tortorici, M. A., Czudnochowski, N., Walls, A. C., Beltramello, M., Silacci-Fregni, C. et al.**, Mapping neutralizing and immunodominant sites on the SARS-CoV-2 spike receptor-binding domain by structure-guided high-resolution serology. *Cell*. 2020. **183**: 1024–1042.e21. Available at: https://www.sciencedirect.com/science/article/pii/S0092867420312344

18 **Gaebler, C., Wang, Z., Lorenzi, J. C. C., Muecksch, F., Finkin, S., Tokuyama, M., Cho, A. et al.**, Evolution of antibody immunity to SARS-CoV-2. *Nature* 2021. **591**: 639–644.

19 **Liu, L., Wang, P., Nair, M. S., Yu, J., Rapp, M., Wang, Q., Luo, Y. et al.**, Potent neutralizing antibodies against multiple epitopes on SARS-CoV-2 spike. *Nature*. 2020. **584**: 450–456.

20 **Greaney, A. J., Loes, A. N., Crawford, K. H. D., Starr, T. N., Malone, K. D., Chu, H. Y. and Bloom, J. D.**, Comprehensive mapping of mutations in the SARS-CoV-2 receptor-binding domain that affect recognition by polyclonal human plasma antibodies. *Cell Host Microbe.* 2021. **29**: 463–476.e6. Available at: https://www.sciencedirect.com/s039cience/article/pii/S1931312821000822

21 **Starr, T. N., Greaney, A. J., Dingens, A. S. and Bloom, J. D.**, Complete map of SARS-CoV-2 RBD mutations that escape the monoclonal antibody LY-CoV555 and its cocktail with LY-CoV016. *Cell. Rep. Med.* 2021. **2**: 100255.

22 **Starr, T. N., Greaney, A. J., Hilton, S. K., Ellis, D., Crawford, K. H. D., Dingens, A. S., Navarro, M. J. et al.**, Deep mutational scanning of SARS-CoV-2 receptor binding domain reveals constraints on folding and ACE2 binding. *Cell*. 2020. **182**: 1295–1310.e20. Available at: https://www.sciencedirect.com/science/article/pii/S0092867420310035.

23 **Greaney, A. J., Starr, T. N., Barnes, C. O., Weisblum, Y., Schmidt, F., Caskey, M., Gaebler, C. et al.**, Mapping mutations to the SARS-CoV-2 RBD that

escape binding by different classes of antibodies. *Nat. Commun.* 2021. **12**: 4196.

24 **Barnes, C. O., Jette, C. A., Abernathy, M. E., Dam, K.-M. A., Esswein, S. R., Gristick, H. B., Malyutin, A. G. et al.**, SARS-CoV-2 neutralizing antibody structures inform therapeutic strategies. *Nature* 2020. **588**: 682–687.

25 **Ge, J., Wang, R., Ju, B., Zhang, Q., Sun, J., Chen, P., Zhang, S. et al.**, Antibody neutralization of SARS-CoV-2 through ACE2 receptor mimicry. *Nat. Commun.* 2021. **12**: 250.

26 **Hansen, J., Baum, A., Pascal, K. E., Russo, V., Giordano, S., Wloga, E., Fulton, B. O. et al.**, Studies in humanized mice and convalescent humans yield a SARS-CoV-2 antibody cocktail. *Science* 2020. **369**: 1010–1014.

27 **Robbiani, D. F., Gaebler, C., Muecksch, F., Lorenzi, J. C. C., Wang, Z., Cho, A., Agudelo, M. et al.**, Convergent antibody responses to SARS-CoV-2 in convalescent individuals. *Nature* 2020. **584**: 437–442.

28 **Rogers, T. F., Zhao, F., Huang, D., Beutler, N., Burns, A., He, W., Limbo, O. et al.**, Isolation of potent SARS-CoV-2 neutralizing antibodies and protection from disease in a small animal model. *Science*. 2020. **369**: 956–963.

29 **Braga, L., Ali, H., Secco, I., Chiavacci, E., Neves, G., Goldhill, D., Penn, R. et al.**, Drugs that inhibit TMEM16 proteins block SARS-CoV-2 spike-induced syncytia. *Nature* 2021. **594**: 88–93.

30 **Sanders, R. W. and Moore, J. P.**, Virus vaccines: proteins prefer prolines. *Cell Host Microbe* 2021. **29**: 327–333.

31 **Prabhakara, C., Godbole, R., Sil, P., Jahnavi, S., Gulzar, S.-J., van, Z. T.S., Sheth, D. et al.**, Strategies to target SARS-CoV-2 entry and infection using dual mechanisms of inhibition by acidification inhibitors. *PLoS Pathog.* 2021. **17**: e1009706.

32 **Karthika, T., Joseph, J., Das, V. R. A., Nair, N., Charulekha, P., Roji, M. D. and Raj, V. S.**, SARS-CoV-2 cellular entry is independent of the ACE2 cytoplasmic domain signaling. *Cells* 2021. 10. Available at: https://www.mdpi.com/2073–4409/10/7/1814

33 **Imai, Y., Kuba, K., Rao, S., Huan, Y., Guo, F., Guan, B., Yang, P. et al.**, Angiotensin-converting enzyme 2 protects from severe acute lung failure. *Nature* 2005. **436**: 112–116.

34 **Clausen, T. M., Sandoval, D. R., Spliid, C. B., Pihl, J., Perrett, H. R., Painter, C. D., Narayanan, A. et al.**, SARS-CoV-2 infection depends on cellular heparan sulfate and ACE2. *Cell* 2020. **183**: 1043–1057.e15. Available at: https://www.sciencedirect.com/science/article/pii/S0092867420312307

35 **Kim, S. Y., Jin, W., Sood, A., Montgomery, D. W., Grant, O. C., Fuster, M. M., Fu, L. et al.**, Characterization of heparin and severe acute respiratory syndrome-related coronavirus 2 (SARS-CoV-2) spike glycoprotein binding interactions. *Antivir Res.* 2020. **181**: 104873. Available at: https://www.sciencedirect.com/science/article/pii/S0166354220302874

36 **Hsieh, C.-L., Goldsmith, J. A., Schaub, J. M., DiVenere, A. M., Kuo, H. C., Javanmardi, K., Le, K. C. et al.**, Structure-based design of prefusion-stabilized SARS-CoV-2 spikes. *Science* 2020. **369**: 1501–1505

37 **Zhou, P., Yang, X.-L., Wang, X.-G., Hu, B., Zhang, L., Zhang, W., Si, H.-R. et al.**, A pneumonia outbreak associated with a new coronavirus of probable bat origin. *Nature* 2020. **579**: 270–273.

38 **Henderson, R., Edwards, R. J., Mansouri, K., Janowska, K., Stalls, V., Gobeil, S. M. C., Kopp, M. et al.**, Controlling the SARS-CoV-2 spike glycoprotein conformation. *Nat. Struct. Mol. Biol.* 2020. **27**: 925–933.

39 **Li, L., Liao, H., Meng, Y., Li, W., Han, P., Liu, K., Wang, Q. et al.**, Structural basis of human ACE2 higher binding affinity to currently circulating Omicron SARS-CoV-2 sub-variants BA.2 and BA.1.1. *Cell* 2022. **185**: 2952–2960.e10. Available at: https://www.sciencedirect.com/science/article/pii/S0092867422007280

40 **Cameroni, E., Bowen, J. E., Rosen, L. E., Saliba, C., Zepeda, S. K., Culap, K., Pinto, D. et al.**, Broadly neutralizing antibodies overcome SARS-CoV-2 Omicron antigenic shift. *Nature* 2022. **602**: 664–670

41 **He, C., He, X., Yang, J., Lei, H., Hong, W., Song, X., Yang, L. et al.**, Spike protein of SARS-CoV-2 Omicron (B.1.1.529) variant has a reduced ability to induce the immune response. *Sig Transduct Target Ther.* 2022. **7**: 119.

42 **Zulli, A., Burrell, L., Buxton, B. and Hare, D.**, ACE2 and AT4R are present in diseased human blood vessels. *Eur. J. Histochem.* 2008. **52**: 39–44.

43 **Fernandes, T., Hashimoto, N. Y. and Oliveira, E. M.**, Characterization of angiotensin-converting enzymes 1 and 2 in the soleus and plantaris muscles of rats. *Braz. J. Med. Biol. Res.* 2010. **43**: 837–842.

44 **Echeverría-Rodríguez, O., Valle-Mondragón, L. D. and Hong, E.**, Angiotensin 1–7 improves insulin sensitivity by increasing skeletal muscle glucose uptake in vivo. *Peptides* 2014. **51**: 26–30.

45 **Xue, X., Mi, Z., Wang, Z., Pang, Z., Liu, H. and Zhang, F.**, High expression of ACE2 on keratinocytes reveals skin as a potential target for SARS-CoV-2. *J. Invest. Dermatol.* 2021. **141**: 206–209.e1.

46 **Sun, S.-H., Chen, Q., Gu, H.-J., Yang, G., Wang, Y.-X., Huang, X.-Y., Liu, S.-S. et al.**, A mouse model of SARS-CoV-2 infection and pathogenesis. *Cell Host Microbe* 2020. **28**: 124–133.e4.

47 **Irvine, D. J., Aung, A. and Silva, M.**, Controlling timing and location in vaccines. *Adv. Drug. Deliv. Rev.* 2020. **158**: 91–115. Available at: https://www.sciencedirect.com/science/article/pii/S0169409x2030065X

48 EMA. *EMEA/H/C/005735/0000 - Assessment report Comirnaty 2021*. Available at: https://www.ema.europa.eu/en/documents/assessment-report/comirnaty-epar-public-assessment-report_en.pdf

49 EMA. *EMEA/H/C/005791/0000 - Assessment report COVID-19 Vaccine Moderna 2021*. Available at: https://www.ema.europa.eu/en/documents/assessment-report/spikevax-previously-covid-19-vaccine-moderna-epar-public-assessment-report_en.pdf

50 EMA. *EMEA/H/C/005675/0000 - Assessment report COVID-19 Vaccine AstraZeneca 2021*. Available at: https://www.ema.europa.eu/en/documents/assessment-report/vaxzevria-previously-covid-19-vaccine-astrazeneca-epar-public-assessment-report_en.pdf

51 **Menni, C., Klaser, K., May, A., Polidori, L., Capdevila, J., Louca, P., Sudre, C. H. et al.**, Vaccine side-effects and SARS-CoV-2 infection after vaccination in users of the COVID Symptom Study app in the UK: a prospective observational study. *Lancet Infect. Dis.* 2021. **21**: 939–949.

52 **Ling, R. R., Ramanathan, K., Tan, F. L., Tai, B. C., Somani, J., Fisher, D. and MacLaren, G.**, Myopericarditis following COVID-19 vaccination and non-COVID-19 vaccination: a systematic review and meta-analysis. *Lancet Respir. Med.* 2022. https://doi.org/10.1016/s2213-2600(22)00059-5

53 **Sidarta-Oliveira, D., Jara, C. P., Ferruzzi, A. J., Skaf, M. S., Velander, W. H., Araujo, E. P. and Velloso, L. A.**. SARS-CoV-2 receptor is co-expressed with elements of the kinin–kallikrein, renin–angiotensin and coagulation systems in alveolar cells. *Sci Rep.* 2020. **10**: 19522.

54 **Gorrell, M. D., Gysbers, V. and McCaughan, G. W.**. CD26: a multifunctional integral membrane and secreted protein of activated lymphocytes. *Scand. J. Immunol.* 2001; **54**: 249–264.

55 **Zhang, P., Gorman, J., Geng, H., Liu, Q., Lin, Y., Tsybovsky, Y., Go, E. P. et al.**, Interdomain stabilization impairs CD4 binding and improves immunogenicity of the HIV-1 envelope trimer. *Cell Host Microbe* 2018; **23**: 832–844.e6. Available at: https://www.sciencedirect.com/science/article/pii/S1931312818302567

56 **Granoff, D. M., Ram, S. and Beernink, P. T.**, Does binding of complement Factor H to the meningococcal vaccine antigen, factor H binding protein,

decrease protective serum antibody responses? *Clin. Vaccine Immunol.* 2013. **20**: 1099–1107.

57 **Hendin, H. E., Lavoie, P.-O., Gravett, J. M., Pillet, S., Saxena, P., Landry, N., D'Aoust, M.-A. et al.**, Elimination of receptor binding by influenza hemagglutinin improves vaccine-induced immunity. *Npj Vaccines* 2022. **7**: 42.

58 **Cohen, A. A., Gnanapragasam, P. N. P., Lee, Y. E., Hoffman, P. R., Ou, S., Kakutani, L. M., Keeffe, J. R. et al.**, Mosaic nanoparticles elicit cross-reactive immune responses to zoonotic coronaviruses in mice. *Science* 2021. **371**: 735–741.

59 **Tian, J.-H., Patel, N., Haupt, R., Zhou, H., Weston, S., Hammond, H., Logue, J. et al.**, SARS-CoV-2 spike glycoprotein vaccine candidate NVX-CoV2373 immunogenicity in baboons and protection in mice. *Nat. Commun.* 2021. **12**: 372.

60 **McKinney, W.**, Data Structures for Statistical Computing in Python. In Millman S van der W and J, (Eds.), *Proc. of the 9th Python in Science Conf (SCIPY2010)*.Vol. 445. 2010: 56–61. DOI: 10.25080/majora-92bf1922-00a

61 **Harris, C. R., Millman, K. J., van der Walt, S., Gommers, R., Virtanen, P., Cournapeau, D., Wieser, E. et al.**, Array programming with NumPy. *Nature* 2020. **585**: 357–362.

62 **Hunter, J. D.**, Matplotlib: A 2D Graphics Environment. *Comput. Sci. Eng.* 2007. **9**: 90–95.

63 **Flyamer, I., Weber, S., Xue, Z., Colin Li, A., vanNeste, C., Espinoza, J. L. et al.**, Phlya/adjustText – a small library for automatically adjustment of text position in Matplotlib plots to minimize overlaps. Available at: https://doi.org/10.5281/zenodo.3924114 [Accessed June 28, 2022].

64 **Amanat, F., Stadlbauer, D., Strohmeier, S., Nguyen, T. H. O., Chromikova, V., McMahon, M., Jiang, K. et al.**, A serological assay to detect SARS-CoV-2 seroconversion in humans. *Nat. Med.* 2020. **26**: 1033–1036.

65 **Lu, M., Chamblee, M., Zhang, Y., Ye, C., Dravid, P., Park, J.-G., Mahesh, K. et al.**, SARS-CoV-2 prefusion spike protein stabilized by six rather than two prolines is more potent for inducing antibodies that neutralize viral variants of concern. *Proc. Natl. Acad. Sci. U.S.A.* 2022. **119**: e2110105119.

66 **Ou, X., Liu, Y., Lei, X., Li, P., Mi, D., Ren, L., Guo, L. et al.**, Characterization of spike glycoprotein of SARS-CoV-2 on virus entry and its immune cross-reactivity with SARS-CoV. *Nat. Commun.* 2020. **11**: 1620.

67 **Du, L., Kou, Z., Ma, C., Tao, X., Wang, L., Zhao, G., Chen, Y. et al.**, A truncated receptor-binding domain of MERS-CoV spike protein potently inhibits MERS-CoV infection and induces strong neutralizing antibody responses: implication for developing therapeutics and vaccines. *PLoS One* 2013. **8**: e81587.

68 **Sharma, S. K., de Val, N., Bale, S., Guenaga, J., Tran, K., Feng, Y., Dubrovskaya, V. et al.**, Cleavage-independent HIV-1 Env trimers engineered as soluble native spike mimetics for vaccine design. *Cell Rep.* 2015. **11**: 539–550. Available at: https://www.sciencedirect.com/science/article/pii/S2211124715003265

69 **Zhou, D., Duyvesteyn, H. M. E., Chen, C.-P., Huang, C.-G., Chen, T.-H., Shih, S.-R., Lin, Y.-C. et al.**, Structural basis for the neutralization of SARS-CoV-2 by an antibody from a convalescent patient. *Nat. Struct. Mol. Biol.* 2020. **27**: 950–958.

70 **Ju, B., Zhang, Q., Ge, J., Wang, R., Sun, J., Ge, X., Yu, J. et al.**, Human neutralizing antibodies elicited by SARS-CoV-2 infection. *Nature* 2020. **584**: 115–119.

71 **Pinto, D., Park, Y.-J., Beltramello, M., Walls, A. C., Tortorici, M. A., Bianchi, S., Jaconi, S. et al.**, Cross-neutralization of SARS-CoV-2 by a human monoclonal SARS-CoV antibody. *Nature* 2020. **583**: 290–295.

72 **Chi, X., Yan, R., Zhang, J., Zhang, G., Zhang, Y., Hao, M., Zhang, Z. et al.**, A neutralizing human antibody binds to the N-terminal domain of the Spike protein of SARS-CoV-2. *Science* 2020. **369**: 650–655.

73 **Corti, D., Zhao, J., Pedotti, M., Simonelli, L., Agnihothram, S., Fett, C., Fernandez-Rodriguez, B. et al.**, Prophylactic and postexposure efficacy of a potent human monoclonal antibody against MERS coronavirus. *Proc. Natl. Acad. Sci. U. S. A.* 2015. **112**: 10473–10478.

74 **Wu, X., Yang, Z.-Y., Li, Y., Hogerkorp, C.-M., Schief, W. R., Seaman, M. S., Zhou, T. et al.**, Rational design of envelope identifies broadly neutralizing human monoclonal antibodies to HIV-1. *Science* 2010. **329**: 856–861.

75 **Lei, C., Qian, K., Li, T., Zhang, S., Fu, W., Ding, M. and Hu, S.**, Neutralization of SARS-CoV-2 spike pseudotyped virus by recombinant ACE2-Ig. *Nat. Commun.*. 2020; **11**: 2070.

76 **Nie, J., Li, Q., Wu, J., Zhao, C., Hao, H., Liu, H., Zhang, L. et al.**, Quantification of SARS-CoV-2 neutralizing antibody by a pseudotyped virus-based assay. *Nat. Protoc.* 2020. **15**: 3699–3715.

77 **Reed, L. J. and Muench, H.**, A simple method of estimating fifty percent endpoints. *Am. J. Epidemiol.* 1938. **27**: 493–497.

78 **Pettersen, E. F., Goddard, T. D., Huang, C. C., Couch, G. S., Greenblatt, D. M., Meng, E. C. and Ferrin, T. E.**, UCSF Chimera—A visualization system for exploratory research and analysis. *J. Comput. Chem.* 2004. **25**: 1605–1612.

79 **Yuan, M., Liu, H., Wu, N. C., Lee, C.-C. D., Zhu, X., Zhao, F., Huang, D. et al.**, Structural basis of a shared antibody response to SARS-CoV-2. *Science* 2020. **369**: 1119–1123.

80 **Lan, J., Ge, J., Yu, J., Shan, S., Zhou, H., Fan, S., Zhang, Q. et al.**, Structure of the SARS-CoV-2 spike receptor-binding domain bound to the ACE2 receptor. *Nature*. 2020. **581**: 215–220.

81 **Saphire, E. O., Parren, P., Pantophlet, R., Zwick, M. B., Morris, G. M., Rudd, P. M., Dwek, R. A. et al.**, Crystal structure of a neutralizing human IgG against HIV-1: a template for vaccine design. *Science* 2001. **293**: 1155–1159.

82 **Xiao, T., Lu, J., Zhang, J., Johnson, R. I., McKay, L. G. A., Storm, N., Lavine, C. L. et al.**, A trimeric human angiotensin-converting enzyme 2 as an anti-SARS-CoV-2 agent. *Nat. Struct. Mol. Biol.*. 2021. **28**: 202–209.

Abbreviations: **2P**: spike-stabilizing substitutions of two prolines · **ACE2**: angiotensin-converting enzyme 2 · **BLI**: biolayer interferometry · **eGFP**: enhanced green fluorescent protein · **fH**: factor H · **HS**: cellular heparin sulfates · **nAbs**: neutralizing antibodies · **NTD**: N-terminal domain of the SARS-CoV-2 spike · **PEI**: polyethylenimine · **PsV**: pseudovirus · **RBD**: receptor binding domain · **RBM**: receptor binding motif

Full correspondence: Dr. Kathrin de la Rosa, Berlin Institute of Health (BIH) at Charité and Max Delbrück Center for Molecular Medicine in the Helmholtz Association (MDC), Berlin 13125, Germany
e-mail: Kathrin.delaRosa@mdc-berlin.de

Received: 27/1/2023
Revised: 27/6/2023
Accepted: 27/6/2023
Accepted article online: 12/7/2023